

Nearby early-type galaxies with ionized gas. The UV emission from GALEX observations^{*}

A. Marino^{1†}, R. Rampazzo², L. Bianchi¹, F. Annibali², A. Bressan^{2,5}, L.M. Buson², M.S. Clemens², P. Panuzzo³, W.W. Zeilinger⁴

¹ *Dept. of Physics and Astronomy, Johns Hopkins University, 3400 North Charles Street, Baltimore, MD 21218 USA*

² *INAF Osservatorio Astronomico di Padova, vicolo dell'Osservatorio 5, I-35122 Padova, Italy*

³ *DSM/Irfu/Service d'Astrophysique, CEA Saclay, 91191 Gif sur Yvette Cedex, France*

⁴ *Institut für Astronomie der Universität Wien, Türkenschanzstraße 17, A-1180 Wien, Austria*

⁵ *SISSA, Via Beirut 4, I-34014 Trieste - Italy*

Accepted. Received

ABSTRACT

We present GALEX far-ultraviolet (FUV, $\lambda_{eff}=1538$ Å) and near-ultraviolet (NUV, $\lambda_{eff}=2316$ Å) surface photometry of 40 early-type galaxies (ETGs) selected from a wider sample of 65 nearby ETGs showing emission lines in their optical spectra. We derive FUV and NUV surface brightness profiles, (FUV-NUV) colour profiles and D_{25} integrated magnitudes. We extend the photometric study to the optical r band from SDSS imaging for 14 of these ETGs. In general, the (FUV-NUV) radial colour profiles become redder with galactocentric distance in both rejuvenated (≤ 4 Gyr) and old ETGs. Colour profiles of NGC 1533, NGC 2962, NGC 2974, NGC 3489, and IC 5063 show rings and/or arm-like structures, bluer than the body of the galaxy, suggesting the presence of recent star formation. Although seven of our ETGs show shell systems in their optical image, only NGC 7135 displays shells in the UV bands. We characterize the UV and optical surface brightness profiles, along the major axis, using a Sersic law. The Sersic law exponent, n , varies from 1 to 16 in the UV bands. S0 galaxies tend to have lower values of n (≤ 5). The Sersic law exponent $n = 4$ seems to be a watershed: ETGs with $n > 4$ tend to have $[\alpha/Fe]$ greater than 0.15, implying a short star-formation time scale. We find a significant correlation between the FUV–NUV colour and central velocity dispersions σ , with the UV colours getting bluer at larger σ . This trend is likely driven by a combined effect of ‘downsizing’ and of the mass-metallicity relation.

Key words: Galaxies: elliptical and lenticular, cD – Galaxies: photometry – Galaxies: fundamental parameters – Galaxies: formation – Galaxies: evolution

1 INTRODUCTION

The importance of ETGs in the context of galaxy formation rests on their evolved nature that makes them the fossil evidence of the process of galaxy evolution. Recent studies at high redshift suggest the existence of a class of objects with very similar morphological, dynamical and stellar population properties to ‘bona fide’, nearby ETGs (see e.g. Franx et al. 2003; Chapman et al. 2004; Treu et al. 2005). This raises the issue of how significant galaxy re-processing has been during the Hubble time, in particular at low red-

shift (i.e. in the range $0 \leq z \leq 1$) where Λ CDM hierarchical models predict that most of the ETG stellar mass was assembled (De Lucia et al. 2006).

The study of the stellar populations in nearby galaxies allows us to trace back with cosmic time the evolutionary history of galaxies. Some recent studies paint a surprising picture for the evolution of ETGs showing that the environment plays a key role in their evolution. From the study of a sample of 124 galaxies, Thomas et al. (2005) find that massive ETGs in low density environments (LDEs) are on average ~ 2 Gyr younger and slightly (~ 0.05 – 0.1 dex) more metal rich than their counterparts in high density environments. Similarly, the study of Clemens et al. (2009), based on a sample of ≈ 14000 ETGs from the Sloan Digital Sky

^{*} Based on GALEX observations: G13-0087 PI R. Rampazzo

[†] E-mail: amarino@pha.jhu.edu

Survey (SDSS), suggests that ETGs in dense environments are $\sim 20\%$ older than those in LDEs. On the other hand, the environment does not affect α -elements enhancement. These results, obtained from the analysis of optical spectra, suggest that the evolutionary process is similar in the cluster and in the field but occurred earlier in more dense environments. ETGs in LDE frequently show signatures of relatively recent evolution, as indicated by the presence of disturbed morphologies (see e.g. Reduzzi et al. 1996; Colbert et al 2001) and of kinematic sub-components (McDermid et al. 2006).

The advent of the Galaxy Ultraviolet Explorer (*GALEX*, Martin et al. (2005)) has contributed to strengthen the idea that recent star formation is often present in ETGs. Through *GALEX* ultraviolet imaging, Schawinski et al. (2007) found that 30% of massive ETGs show ongoing star formation and that this fraction is higher in LDEs. Rogers et al. (2007) concluded that ETGs in low density environments are less likely to present weak episodes of recent star formation than their high-density counterparts. *GALEX* studies of ETGs with shell structures are of particular relevance, since these features, believed to be ‘bona fide’ signatures of recent accretion/merging events, characterize a significant fraction ($\approx 16.5\%$) of field ETGs (Malin & Carter 1983). Combined analyses of Lick line-strength indices (e.g. $Mg2$, $H\beta$, $H_{\gamma A}$, $H_{\delta A}$) and UV colours, revealed the presence of recent star formation in shell galaxies (Rampazzo et al. 2007; Marino et al. 2009). Similar results have been recently obtained by Jeong et al. (2009) for a *SAURON* galaxy sample. They determined the UV Fundamental Plane and suggested that the dominant fraction of the tilt and the scatter of this plane is due to the presence of young stars in preferentially low mass ETGs.

This is the fifth paper of a series dedicated to the study of ETGs with emission lines (Rampazzo et al. (2005) hereafter Paper I; Annibali et al. (2006) hereafter Paper II; Annibali et al. (2007) hereafter Paper III; Annibali et al. (2010) hereafter Paper IV). Our program considers 65 ETGs mainly located in groups and low density environments (LDEs). In paper III, we showed that the ETGs of our sample have a large age spread, with luminosity-weighted ages ranging from 1 Gyr to a Hubble time. Luminosity-weighted ages younger than 5 Gyr are always associated with the galaxies residing in the lowest density environments. We suggest that such young ages are due to ‘rejuvenation’ episodes, which do not involve more than 25% of the total galaxy stellar mass. In Paper IV we investigated the nature of the ionization mechanism through standard emission-line diagnostic diagrams (e.g. $\log [OIII]/H\beta$ vs. $\log [NII]/H\alpha$). The majority of our ETGs are classified as LINERs. Galaxies classified as Seyferts in our sample tend to have very young (< 5 Gyr) mean ages, supporting that star formation and AGN phenomena co-exist (see e.g. Terlevich et al. 1990; Wada 2004). The gas oxygen abundance, derived through the emission lines, gives systematically lower values than that of stars. A possible explanation is that the gas has an external origin, e.g. derived from the accretion of a metal poorer companion.

We present in this paper *GALEX* FUV and NUV surface photometry of 40 ETGs. The UV wavelengths are particularly sensitive to young populations, and thus ideal to characterize any recent star formation. The paper is organized as follows. In Section 2 we describe the sample. Sec-

tions 3 presents the *GALEX* UV observations, the data reduction and the comparison of our results with the literature. In Section 4 we present our results. We discuss the galaxy morphological peculiarities, the shape of the surface brightness profiles, the UV radial colour profiles. In Appendix A we summarize, for the individual galaxies, the UV and optical photometric properties, as well as the kinematic and morphological peculiarities. In Appendix B we include the *r*-band surface photometry obtained for a subset of 14 galaxies from SDSS data.

2 SAMPLE

A sample of 40 galaxies is selected from a wider sample of 65 ETGs (see Paper I and II). Table 1 reports the main properties of the sample. Column (1) gives the galaxy identification; column (2) provides the galaxy morphological classification according to RC3 (de Vaucouleurs et al. 1991). Only in a few cases does the RC3 differ from that of the RSA (Sandage & Tammann 1987): NGC 4552, NGC 5846, NGC 6958 and NGC 7192 are classified as S0 in RSA and as E in RC3. Column (3) gives the galaxy systemic velocity, V_{hel} , which is lower than ~ 5000 km s $^{-1}$ in all cases. For galaxies with a heliocentric systemic velocity lower than 3000 km s $^{-1}$ we adopt the distances (column 4) provided by Tully (1988). For larger velocities, distances assume a Hubble Constant of $H_0 = 75$ km s $^{-1}$ Mpc $^{-1}$. Columns (5) and (6) provide the optical effective radius, r_e , i.e the radius of the circular aperture encircling half of the total galaxy optical light, and the average ellipticity, as obtained from RC3 and *HYPERCAT*. In column (7) we report the galaxy central velocity dispersion, within an aperture of 1/8 of the effective radius. Cappellari et al. (2006) has investigated the relation between galaxy mass-to-light ratio and the line-of-sight component of the velocity dispersion. They provide relations (their equation 7 and 10) which allow a direct transformation from the measured velocity dispersion to galaxy mass. According to the above formulae, the quoted velocity dispersion, that ranges from ≈ 130 to 340 km s $^{-1}$, indicate that our galaxies cover a large range in masses (roughly $3 \times 10^{10} - 9 \times 10^{11} M_{\odot}$).

The luminosity-weighted ages as derived in Paper III are given in column (8); they range from 1.7 ± 0.1 Gyr (NGC 3489) to 14.5 ± 4.2 Gyr (NGC 1052). Elliptical galaxies are on average older than lenticulars. A definite trend of increasing metallicity (column 9) and $[\alpha/Fe]$ (column 10) with the velocity dispersion is observed, testifying that the chemical enrichment was more efficient and the duration of the star formation shorter in more massive galaxies. These two relations do not depend on the galaxy morphological type.

Nebular emission lines are commonly found in the inner regions of ETGs: in the optical, the fractions of documented detection in different samples are 55%-60% (Phillips et al. 1986), 72% (ellipticals, E) -85% (lenticulars, S0) (Macchetto et al. 1996), 66%(E) -83% (S0) (Sarzi et al. 2006), and 52% (Yan et al. 2006). Concerning a possible environmental effect on the presence of emission lines in ETGs, Grossi et al. (2009), in a sample of 62 ETGs in low density environments, found that 44% of the luminous ETGs ($M_B < -17$) are detected in HI (i.e. 10 times more fre-

Table 1. The sample overview

Ident.	RC3	V_{hel} [km s ⁻¹]	Dist. [Mpc]	r_e [arcsec]	ϵ	$\sigma_{re}/8$ [km s ⁻¹]	Age [Gyr]	Z	[α /Fe]	Activity Class	ρ_{xyz} [Gal. Mpc ⁻³]
NGC 128	S0 pec sp	4227	56.4	17.3	0.67	183	9.7 ± 1.7	0.024 ± 0.004	0.16 ± 0.03	LIN	
NGC 777	E1	5040	67.2	34.4	0.21	317	5.4 ± 2.1	0.045 ± 0.020	0.28 ± 0.10	Sy/LIN	
NGC 1052	E4	1475	17.8	33.7	0.28	215	14.5 ± 4.2	0.032 ± 0.007	0.34 ± 0.05	LIN	0.49
NGC 1209	E6:	2619	32.9	18.5	0.52	240	4.8 ± 0.9	0.051 ± 0.012	0.14 ± 0.02	LIN	0.13
NGC 1380	SA0	1844	16.9	20.3	0.41	240	4.4 ± 0.7	0.038 ± 0.006	0.24 ± 0.02	LIN	1.54
NGC 1389	SAB(s)0:-	986	16.9	15.0	0.37	139	4.5 ± 0.6	0.032 ± 0.005	0.08 ± 0.02	IN	1.50
NGC 1407	E0	1766	21.6	70.3	0.07	286	8.8 ± 1.5	0.033 ± 0.005	0.32 ± 0.03	IN	0.42
NGC 1426	E4	1443	16.8	25.0	0.34	162	9.0 ± 2.5	0.024 ± 0.005	0.07 ± 0.05	IN	0.66
NGC 1453	E2	3906	52.1	25.0	0.17	289	9.1 ± 2.8	0.034 ± 0.009	0.22 ± 0.05	LIN	
NGC 1521	E3	4165	55.5	25.5	0.35	235	3.2 ± 0.4	0.037 ± 0.006	0.09 ± 0.02	LIN	
NGC 1533	SB0-	773	13.4	30.0	0.19	174	11.9 ± 6.9	0.023 ± 0.020	0.21 ± 0.10	LIN	0.89
NGC 1553	SA(r)0	1280	13.4	65.6	0.38	180	4.8 ± 0.7	0.031 ± 0.004	0.10 ± 0.02	LIN	0.97
NGC 2911	SA(s)0: pec	3131	41.7	50.9	0.32	235	5.7 ± 2.0	0.034 ± 0.019	0.25 ± 0.10	LIN	
NGC 2962	RSAB(rs)0+	2117	30.6	23.3	0.37						0.15
NGC 2974	E4	1890	28.5	24.4	0.37	220	13.9 ± 3.6	0.021 ± 0.005	0.23 ± 0.06	LIN	0.26
NGC 3258	E1	2778	37.5	30.0	0.13	271	4.5 ± 0.8	0.047 ± 0.013	0.21 ± 0.03	Comp.	0.72
NGC 3268	E2	2818	37.5	36.1	0.24	227	9.8 ± 1.7	0.023 ± 0.004	0.34 ± 0.04	LIN	0.69
NGC 3489	SAB(rs)0+	693	6.4	20.3	0.37	129	1.7 ± 0.1	0.034 ± 0.004	0.05 ± 0.02	Sy/LIN	0.39
NGC 3607	SA(s)0:	934	19.9	43.4	0.11	220	3.1 ± 0.5	0.047 ± 0.012	0.24 ± 0.03	LIN	0.34
NGC 3818	E5	1701	25.1	22.2	0.36	191	8.8 ± 1.2	0.024 ± 0.003	0.25 ± 0.03		0.20
NGC 3962	E1	1822	28.0	35.2	0.22	225	10.0 ± 1.2	0.024 ± 0.003	0.22 ± 0.03	LIN	0.32
NGC 4374	E1	1060	16.8	50.9	0.13	282	9.8 ± 3.4	0.025 ± 0.010	0.24 ± 0.08	LIN	3.99
NGC 4552	E	322	16.8	29.3	0.06	264	6.0 ± 1.4	0.043 ± 0.012	0.21 ± 0.03	Comp.	2.97
NGC 4697	E6	1241	23.3	72.0	0.32	174	10.0 ± 1.4	0.016 ± 0.002	0.14 ± 0.04	LIN	0.60
NGC 5011	E1-2	3104	40.9	23.8	0.15	249	7.2 ± 1.9	0.025 ± 0.008	0.25 ± 0.06	LIN	0.27
NGC 5044	E0	2704	38.9	82.3	0.11	239	14.2 ± 10.	0.015 ± 0.022	0.34 ± 0.17	LIN	0.38
NGC 5363	[S03(5)]	1138	22.4	36.1	0.34	199	12.1 ± 2.3	0.020 ± 0.004	0.16 ± 0.05	LIN	0.28
NGC 5638	E1	1676	28.4	28.0	0.11	165	9.1 ± 2.3	0.024 ± 0.008	0.24 ± 0.05	IN	0.79
NGC 5813	E1-2	1972	28.5	57.2	0.15	239	11.7 ± 1.6	0.018 ± 0.002	0.26 ± 0.04	LIN	0.88
NGC 5831	E3	1656	28.5	25.5	0.15	164	8.8 ± 3.5	0.016 ± 0.011	0.21 ± 0.09	IN	0.83
NGC 5846	E0+	1709	28.5	62.7	0.07	250	8.4 ± 1.3	0.033 ± 0.005	0.25 ± 0.03	LIN	0.84
NGC 6868	E2	2854	35.5	33.7	0.19	277	9.2 ± 1.8	0.033 ± 0.006	0.19 ± 0.03	LIN	0.47
NGC 6958	E+	2652	35.4	19.8	0.15	223	3.0 ± 0.3	0.038 ± 0.006	0.20 ± 0.03	Sy/LIN	0.12
NGC 7079	SB(s)0	2670	33.9	19.8	0.32	155	6.7 ± 1.1	0.016 ± 0.003	0.21 ± 0.05	LIN	0.19
NGC 7135	SA0- pec	2718	34.7	31.4	0.31	231	2.2 ± 0.4	0.047 ± 0.010	0.46 ± 0.04	LIN	0.32
NGC 7192	E+:	2904	35.6	28.6	0.15	257	5.7 ± 2.0	0.039 ± 0.015	0.09 ± 0.05	LIN	0.28
NGC 7332	S0 pec sp	1207	18.2	14.7	0.42	136	3.7 ± 0.4	0.019 ± 0.002	0.10 ± 0.03		0.12
IC 1459	E	1659	20.0	34.4	0.28	311	8.0 ± 2.2	0.042 ± 0.009	0.25 ± 0.04	LIN	0.28
IC 4296	E	3762	50.2	41.4	0.17	340	5.2 ± 1.0	0.044 ± 0.008	0.25 ± 0.02	LIN	
IC 5063	SA(s)0+:	3402	45.4	26.7	0.28	160				Sy	

Notes: See text for a detailed explanation of single columns. The age, metallicity and the α -enhancement obtained from the Lick line-strength indices analysis, are obtained from Paper III. The activity class is discussed in Paper IV. We used here the following notation: LIN = LINER; Sy = Syfert like emission; Comp. = spectra can be due to either 1) a combination of star formation and a Seyfert nucleus, or 2) a combination of star formation and LINER emission (Kewley et al. 2006), IN = either faint or no emission lines.

quently than in the Virgo cluster), 60% of which show emission line ratios typical of star-forming galaxies. Optical emission lines are detected in 89% of our original sample of 65 ETGs (Paper IV). For the sample of 40 ETGs studied in this paper, the detection drops to 82%. Incidence and strength of line emission do not correlate either with the E/S0 classification, or with the fast/slow rotator classification.

By means of optical emission line ratios (e.g., [OIII] λ 5007/H β and [NII] λ 6584/H α , Baldwin et al. (1981)), we have shown that for the majority of our ETGs the emission is “indistinguishable” from that of low-ionization nuclear emission-line regions (LINERs, Heckman (1980)) in agreement with other studies of ETGs (see e.g. Phillips et al. 1986; Goudfrooij 1998; Kewley et al. 2006). The activity class, as derived in Paper IV from optical emission line diagnostic diagrams, is given in column 11 of Table 1.

The richness of the environment in which our ETGs are located is well described by the parameter ρ_{xyz} (column 12 of Table 1) provided by Tully (1988) in the *Nearby Galaxy Catalog*. It represents the density of galaxies brighter than B=-16 mag in the vicinity of each galaxy in Mpc⁻³. The

galaxies of our sample are mainly located in low density environments. The local density around our galaxies varies from $\rho_{xyz} \approx 0.1$, characteristic of nearly isolated galaxies, to $\rho_{xyz} \approx 4$, which is characteristic of dense galaxy regions in the Virgo cluster. For comparison, in the Tully (1988) catalogue NGC 1380 and NGC 1389, Fornax cluster members, have values of $\rho_{xyz}=1.54$ and 1.50 respectively. Thus our sample, although biased towards low density environments, contains a fraction of galaxies in relatively dense environments.

3 OBSERVATIONS AND DATA REDUCTION

The UV imaging was obtained with GALEX (Martin et al. 2005; Morrissey et al. 2007) in two ultraviolet bands, FUV (1344 – 1786 Å) and NUV (1771 – 2831 Å). The instrument has a very wide field of view (1.25 degrees diameter) and a spatial resolution $\approx 4''2$ and $5''3$ FWHM in FUV and NUV respectively, sampled with $1''5 \times 1''5$ pixels (Morrissey et al. 2007).

The sample we analyze is composed of 16 ETGs ob-

served in our Cycle 3 proposal (ID GI3-0087 PI R. Rampazzo) and 24 ETGs taken from the public *GALEX* archive (see Table 2). The exposure times for most of our sample are ~ 1500 seconds (limiting magnitude in FUV/NUV of $\sim 22.6/22.7$ AB mag (Bianchi 2009). NGC 1389 and NGC 5363 have exposure times ~ 10 times longer (~ 2.5 mag fainter limit). For each galaxy, in Figure 1 we show the *GALEX* FUV and NUV images and a false colour composite image.

Additional *GALEX* observations with exposure times of about 100 seconds exist for the following sub-set of the Paper I plus Paper II samples: NGC 1947, NGC 5193, NGC 6721, NGC 6758, NGC 7007 and NGC 7377 but were not considered in the present paper, in order to have an homogeneous flux limit.

We used background-subtracted FUV and NUV *GALEX* intensity images to perform photometry. Table 3 lists the FUV and NUV magnitudes in the AB system of the ETG sample within $r_e/4$, $r_e/8$ and D_{25} apertures, where r_e and D_{25} are the optical effective radius (see Table 1) and the diameter of the isophote at $\mu_B=25$ mag arcsec $^{-2}$ respectively (taken from HYPERLEDA). The D_{25} ellipses are shown in Figure 1. FUV and NUV magnitudes were computed as $m_{UV} = -2.5 \times \log CR_{UV} + ZP$, where CR is the dead-time-corrected flat-fielded count rate, and the zero points $ZP=18.82$ and 20.08 mag in FUV and NUV respectively (Morrissey et al. 2007). FUV and NUV magnitudes and photometric errors were determined from the original un-smoothed images, after manually subtracting foreground stars. In order to estimate the errors on UV magnitudes, we propagated the Poisson statistical errors on source and background counts. Background counts were computed measuring the background images provided by the *GALEX* pipeline in the same D_{25} aperture of the galaxy. In addition to the statistical error, we added an uncertainty to account for systematic inaccuracies in the zero point of the absolute calibration of 0.05 and 0.03 magnitudes for FUV and NUV respectively (Morrissey et al. 2007).

The comparison between our D_{25} magnitudes and those of Gil de Paz et al. (2007) shows general agreement. Discrepant measurements are found only in the FUV for NGC 5813 ($D_{25our}-D_{25GdP}=0.42$), NGC 777 (0.29) and NGC 5638 (0.20). For these objects, the D_{25} sizes adopted by Gil de Paz et al. (2007), taken from RC3 slightly differ from ours, taken from Hyperleda, and may account for the discrepancies.

The surface photometry was carried out using the ELLIPSE fitting routine in the STSDAS package of IRAF. ELLIPSE computes a Fourier expansion for each successive isophote (Jedrzejewski 1987), resulting in photometric surface profiles. We masked the foreground objects in the regions where we evaluated the surface brightness profiles. Surface photometry was corrected for galactic extinction assuming Milky Way dust with $R_V=3.1$ (Cardelli et al. 1989), $A_{FUV}/E(B-V)=8.376$ and $A_{NUV}/E(B-V)=8.741$. The UV radial profiles are truncated when the uncertainty in the surface brightness exceeds 0.3 mag arcsec $^{-2}$. The UV limiting surface brightness is ~ 28 AB mag/arcsec 2 . Radial (FUV-NUV) colour profiles generally become redder from the centre to the periphery of the galaxy. Significant deviation from this general behaviour is found in the galaxies showing ring and/or arm-like features.

Table 2. Journal of the *GALEX* observations

Ident.	FUV Exp. Time [sec]	NUV Exp. Time [sec]	Observing program
NGC 128	1499	1499	GI3_089001
NGC 777	1992	1992	NGA_NGC777
NGC 1052	2982	3834	NGA_NGC1052
NGC 1209	1637	2940	GI3_087001
NGC 1380	1646	1646	NGA_NGC1380
NGC 1389	17543	18602	FORNAX_MOS08
NGC 1407	1575	1575	NGC_NGC1407
NGC 1426	1693	1693	GI3_087002
NGC 1453	3382	5301	GI3_087003
NGC 1521	1662	11746	GI1_047024
NGC 1533	1520	3152	GI3_087004
NGC 1553	2016	2016	NGA_NGC1553
NGC 2911	1605	1605	GI3_079009
NGC 2962	2297	2297	MISWZN09_24136_0336
NGC 2974 ^{1,2}	2657	2657	GI1_109006
NGC 3258	2223	2223	GI3_087006
NGC 3268	2223	2223	GI3_087006
NGC 3489	1642	1642	GI3_087007
NGC 3607	2468	2468	GI1-079016
NGC 3818	1166	1166	GI3_087008
NGC 3962	2098	2098	GI3_087009
NGC 4374 ²	1606	2978	NGC_Virgo_MOS10
NGC 4552 ²	1600	4770	NGA_Virgo_MOS03
NGC 4697	1696	1696	GI4_085003
NGC 5011	1578	1578	GI3_087010
NGC 5044	1696	1696	GI3_087011
NGC 5363	16947	18451	PS_VISTA_MOS04
NGC 5638	1704	1704	MISDR1_33739_0535
NGC 5813 ²	2539	2539	GI3_041009
NGC 5831 ²	2372	5335	GI1_109008
NGC 5846 ²	1479	1479	GI3_041010
NGC 6868	1700	1700	GI3_087012
NGC 6958	3094	3094	NGA_NGC6958
NGC 7079	1708	1709	GI3_087013
NGC 7135 ³	1693	1693	GI1_059005
NGC 7192	1754	1754	GI3_087014
NGC 7332	1807	1807	GI3_079031
IC 1459	1678	1678	GI1_093001
IC 4296	1701	3365	GI3_087015
IC 5063	2958	2958	GI3_087016

We indicate the ETGs for which a detailed UV surface photometry has been performed: ¹ Jeong et al. (2007); ² Jeong et al. (2009); ³ Rampazzo et al. (2007).

In Figure 2 we present the *GALEX* FUV and NUV surface brightness profiles (left panels) along the major axis and the (FUV-NUV) radial colour profiles. A short description of individual galaxies is given in the Appendix A.

Six ETGs were also measured by Jeong et al. (2009). There are no systematic differences among their and our measures. The largest difference is found for NGC 2974: the average difference in the FUV and the NUV surface brightness is $\langle (FUV_{Jeong09} - FUV_{our}) \rangle = 0.23 \pm 0.12$ mag and $\langle (NUV_{Jeong09} - NUV_{our}) \rangle = 0.17 \pm 0.10$ mag, likely due to the estimate of the background, determined following different approaches by the two studies. For the other galaxies the average differences are generally smaller, sometimes lower than formal errors. In particular: NGC 4374 $\langle (FUV_{Jeong09} - FUV_{our}) \rangle = 0.08 \pm 0.10$ and $\langle (NUV_{Jeong09} - NUV_{our}) \rangle = 0.01 \pm 0.05$; NGC 4552 $\langle (FUV_{Jeong09} - FUV_{our}) \rangle = -0.14 \pm 0.14$ and $\langle (NUV_{Jeong09} - NUV_{our}) \rangle = -0.04 \pm 0.07$; NGC 5813 $\langle (FUV_{Jeong09} - FUV_{our}) \rangle = 0.11 \pm 0.08$ and $\langle (NUV_{Jeong09} - NUV_{our}) \rangle = 0.11 \pm 0.07$; NGC 5831 $\langle (FUV_{Jeong09} - FUV_{our}) \rangle = -0.18 \pm 0.22$ and $\langle (NUV_{Jeong09} - NUV_{our}) \rangle = -0.01 \pm 0.09$; NGC 5846 $\langle (FUV_{Jeong09} - FUV_{our}) \rangle = 0.01 \pm 0.07$ and $\langle (NUV_{Jeong09} - NUV_{our}) \rangle = 0.02 \pm 0.04$.

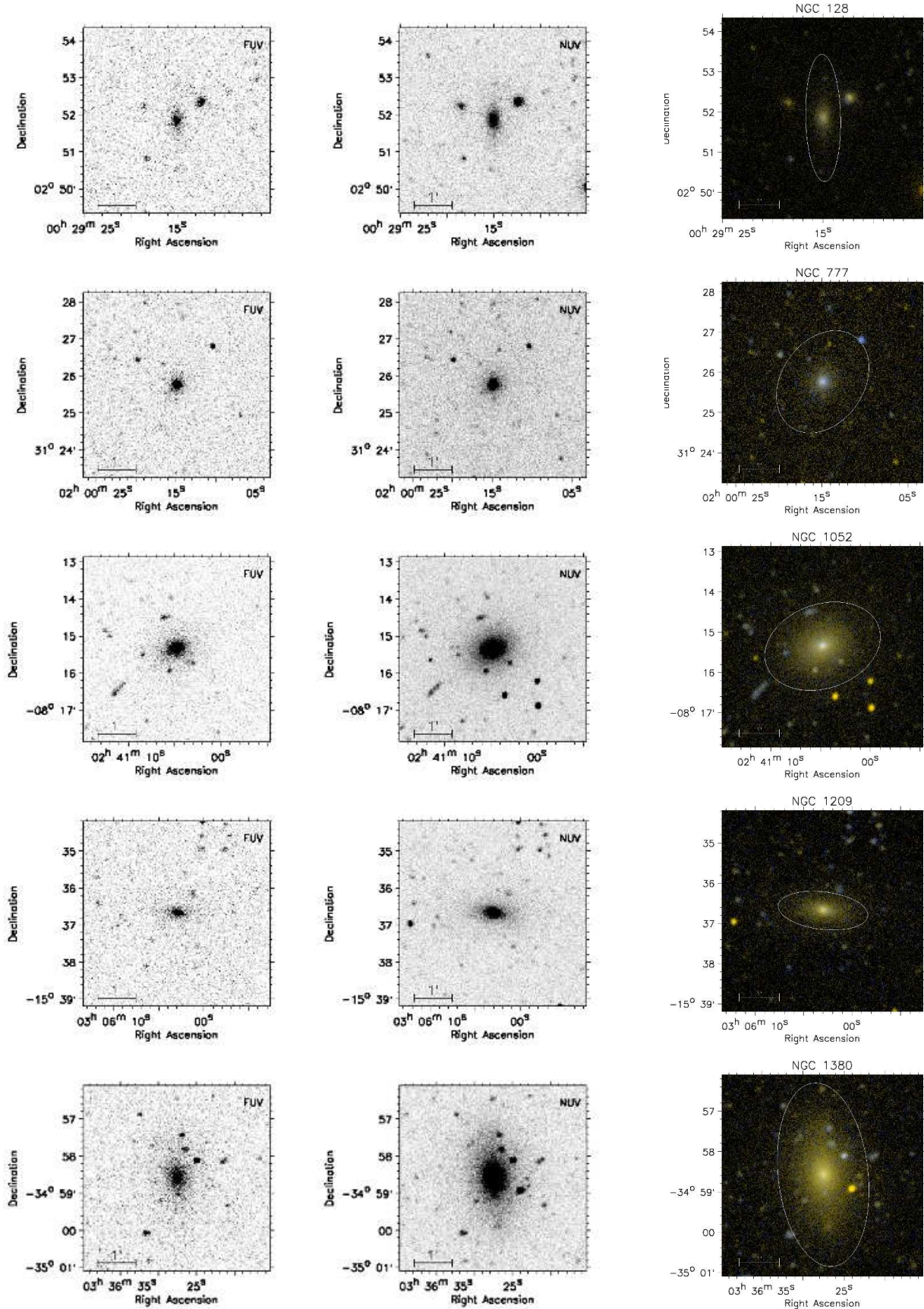


Figure 1. Left and middle panels: *GALEX* FUV and NUV background subtracted images of the sample. Right panel: false colour images (FUV Blue; NUV yellow). Ellipses mark the optical D₂₅ diameter, within which we measure the NUV and FUV integrated magnitudes. Figure 1 is available in its entirety in the the online version of the Journal. A small portion is shown here for guidance.

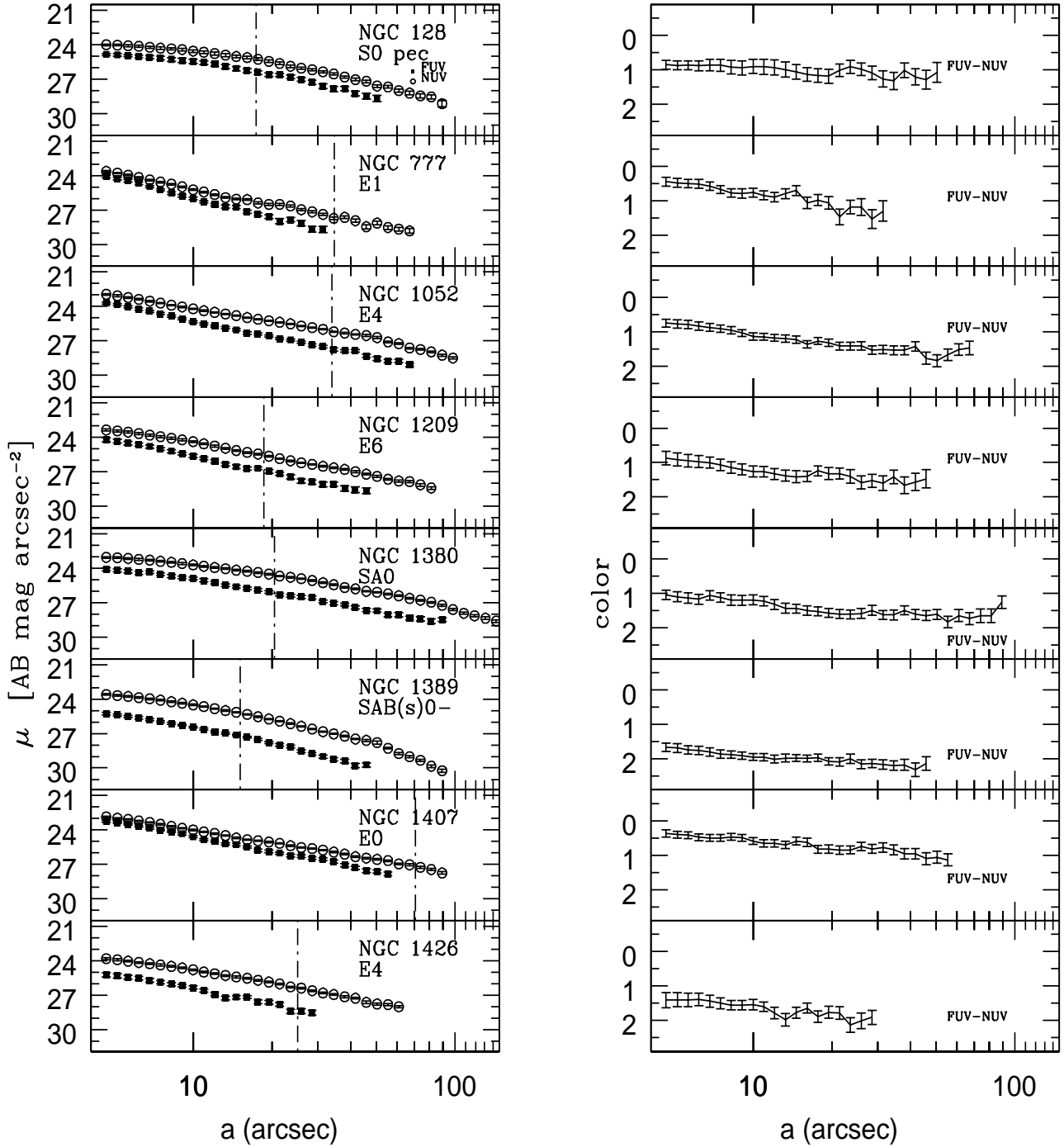


Figure 2. From top to bottom: (left panels) Luminosity profiles along the semi-major axis of the fitted ellipse in the *GALEX* FUV and NUV bands. The vertical dot-dashed lines indicate the optical effective radius (see Table 1). (right panel) Radial (FUV-NUV) colour profile v.s. semi-major axis.

In addition to the UV data, we used optical SDSS archival data (Adelman et al. 2008) in the u [2980-4130 Å], g [3630-5830 Å], r [5380-7230 Å], i [6430-8630 Å] and z [7730-11230 Å] bands available for 14 ETGs in our sample (see Figure B.1 in Appendix B for SDSS composite images). We

registered the SDSS images (corrected frames with the ‘soft bias’ of 1000 subtracted) to the corresponding *GALEX* NUV image using the IRAF tool `sregister`. We computed the

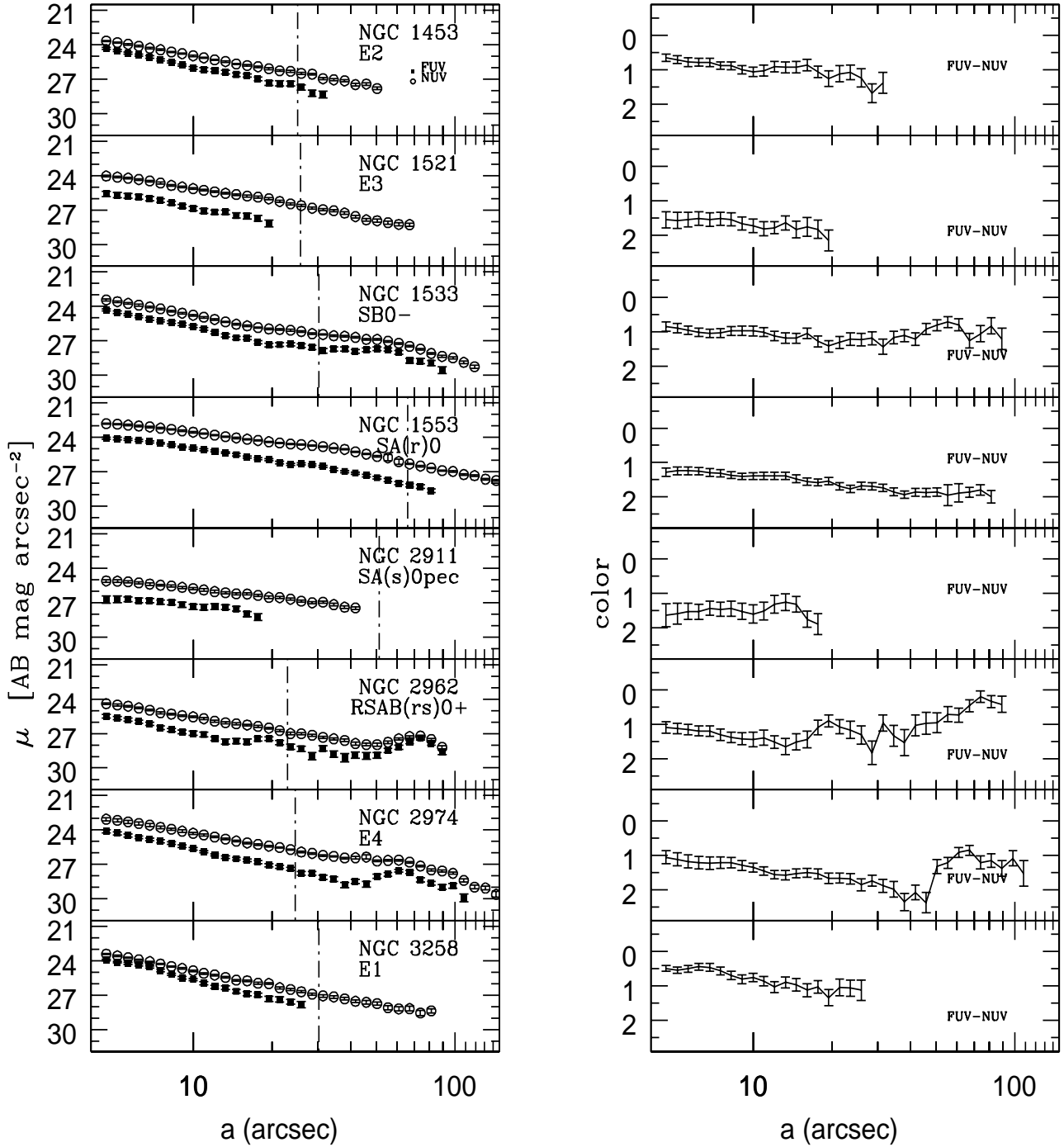


Figure 2. Continued.

SDSS magnitudes in the r band within $r_e/8$ and D_{25}^1 (Table

¹ We converted SDSS counts to magnitudes following the recipe provided in <http://www.sdss.org/df7/algorithms/fluxcal.html> #counts2mag

3). Figure B1, in Appendix B, shows the surface brightness profiles in the r band and the (FUV- r) and (NUV- r) colour profiles. The integrated optical photometry will be used in Section 4.6 to investigate the UV-optical colour magnitude relation for the sub-sample of 14 ETGs.

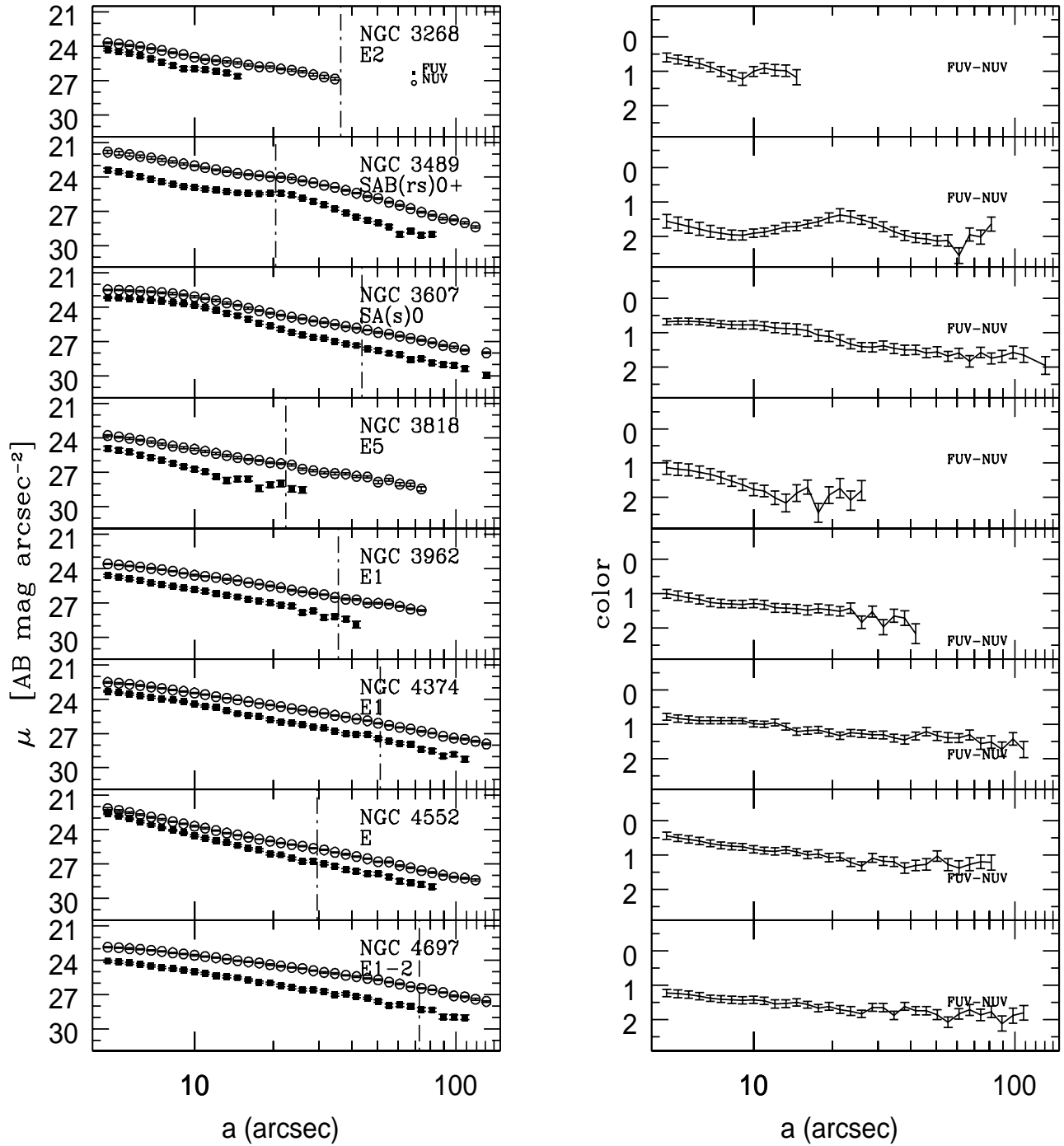


Figure 2. Continued.

4 RESULTS AND DISCUSSION

4.1 FUV and NUV morphology

In general, the FUV emission is less extended than the NUV emission (see e.g. Gil de Paz et al. 2007; Jeong et al. 2007; Rampazzo et al. 2007; Jeong et al. 2009).

The barred lenticular galaxies NGC 1533, NGC 2962 and NGC 3489 show rings and loops. NGC 2974, classified in RC3 as E4, likely has a small scale and possibly a large scale bar. Krajnović et al. (2005) found, with SAURON observations, the existence of non-axisymmetric perturbations consistent with the presence of inner bars.

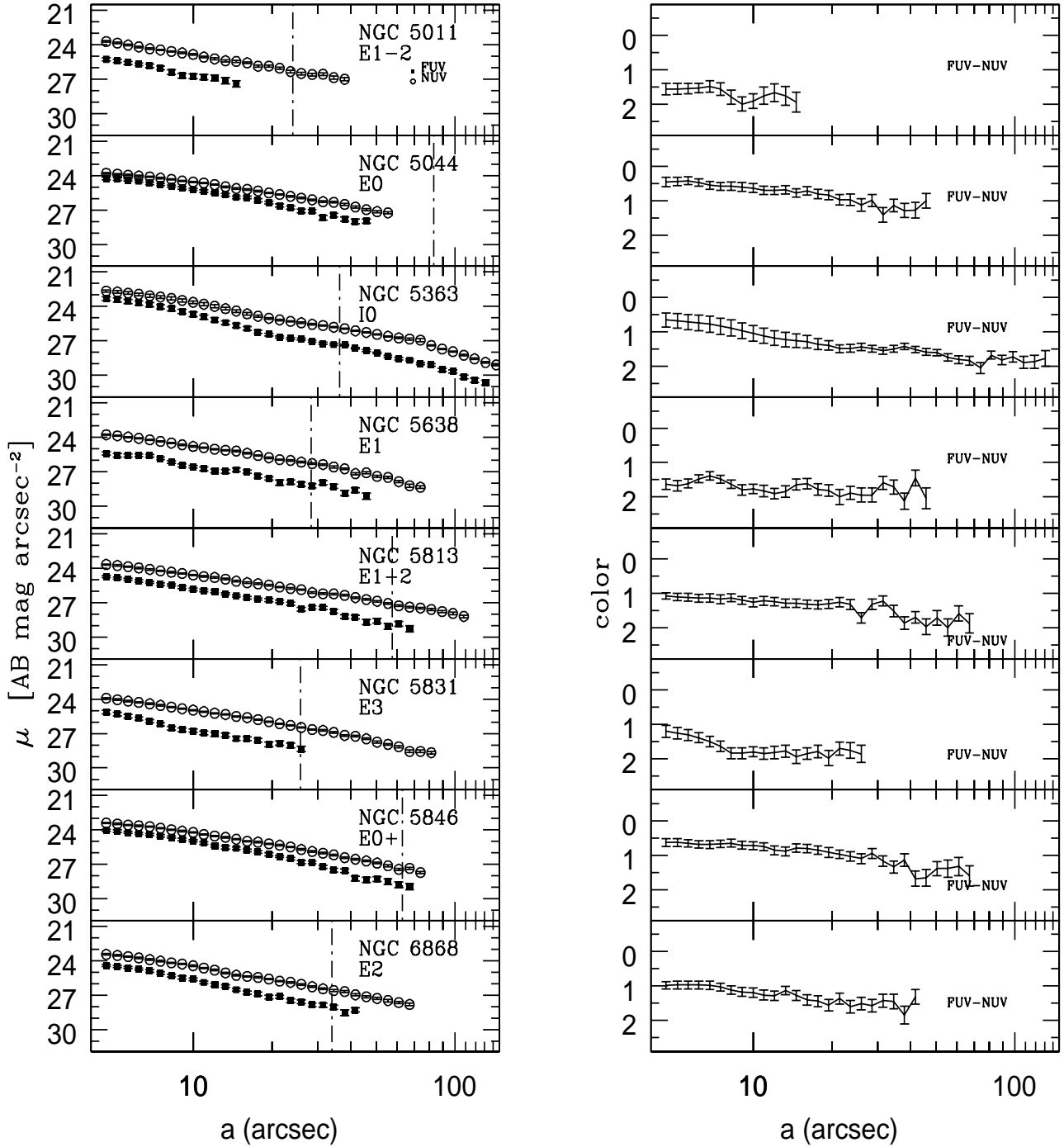


Figure 2. Continued.

According to the different statistical estimates, rings are observed in a significant fraction, up to 20-30%, of lenticulars and spirals (e.g. Thilker et al. 2007; Bianchi et al. 2007) and are closely associated with non-axisymmetric structures like bars, ovals or triaxial bulges. This fact is traditionally explained with orbits crowding and gas accumulation at the

Lindblad resonances (see e.g. Buta & Combes 1996). This kind of rings has an internally driven origin and differs both from rings generated by galaxy-galaxy interaction, e.g. head-on collisional rings, (see e.g. Athanassoula 2009) and from merging events, e.g. polar rings (Marino et al. 2009).

In gas rich systems the bar drives gas inflow due

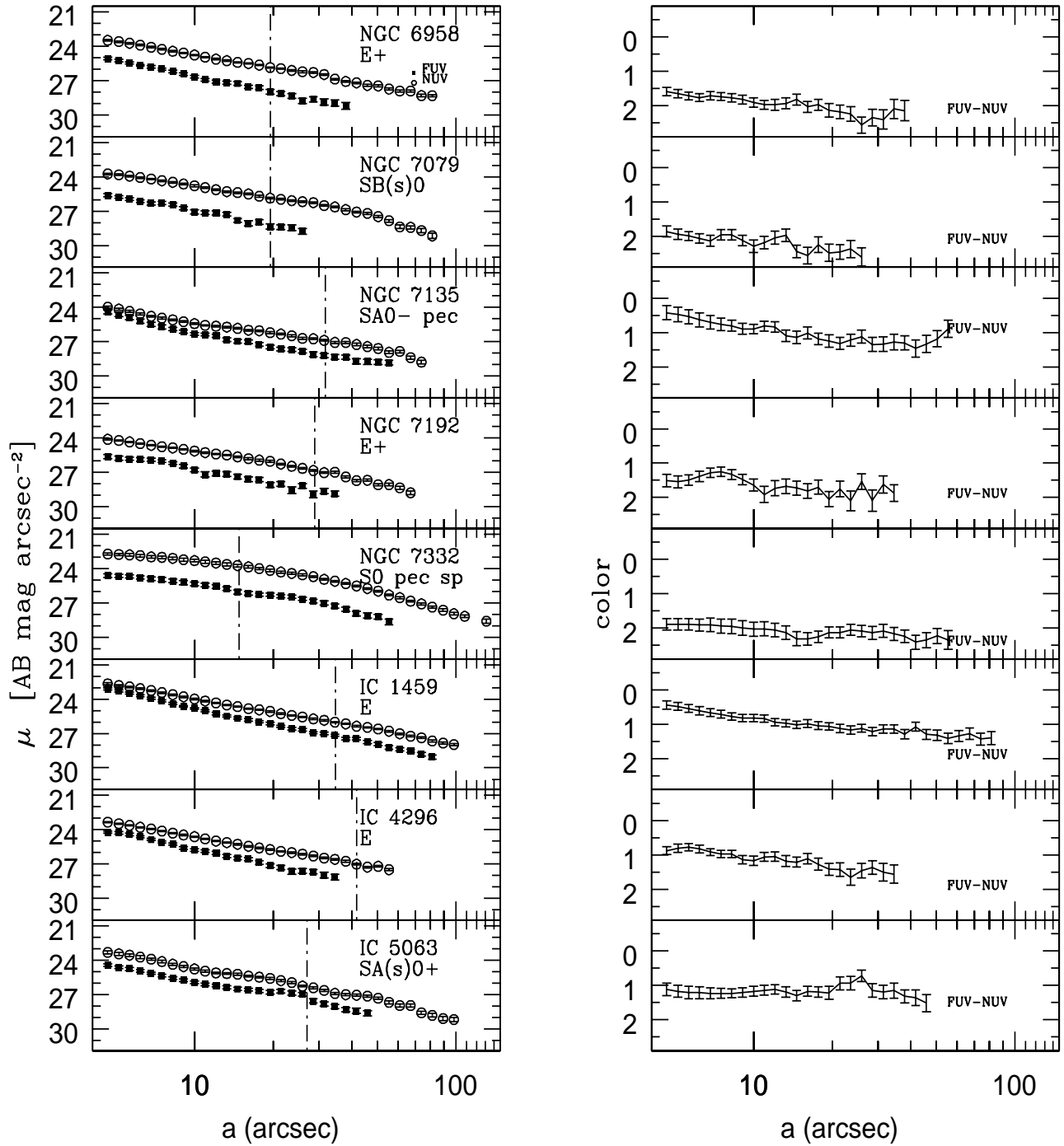


Figure 2. Continued.

to its gravity torque and could then trigger nuclear star formation and/or AGN activity (see e.g. Bournaud et al. 2005). This does not seem the case of both the nuclei of NGC 1533 and of NGC 2974 which appear quite old with a luminosity-weighted age >10 Gyr (see Table 1). In the case of NGC 2974, a possible explanation is suggested

by the complex gas kinematics evidenced by the work of Krajnović et al. (2005) which likely prevents star formation.

The NUV as well as the FUV emission in the ring structures are not uniform and present knotty regions. Arm-like structures departing from the ring are clearly visible in NGC 2974 as well as in NGC 2962. Sandage & Brucato

(1979) suggest the presence of a weak spiral pattern in the outer lense in NGC 1533. In the SW of the NUV image a spiral pattern, departing from the ring, is visible. The NUV and FUV images show the presence of a nucleus while the bar is not clearly visible. The ring structure is not as regular as in the NIR band images (and residuals) shown by Laurikainen et al. (2006) but is marked by bright knots in the NE visible also in the FUV band.

A complex loop structure is evident in the unbarred lenticular Seyfert galaxy IC 5063. This structure, seen nearly edge-on, seems not confined to a plane.

Prominent dust structures are clearly visible in NGC 5363 and NGC 7192 (Figure 1).

There are seven shell galaxies in the sample, namely NGC 1553, NGC 2974, NGC 4552, NGC 6958, NGC 7135, NGC 7192 and IC 1459 (Malin & Carter 1983; Tal et al. 2009). Only NGC 7135 shows the peculiar shell structure visible in the optical image, enhanced by the higher contrast provided by the UV sensitivity to the younger stellar population (Rampazzo et al. 2007). In particular, the FUV image shows a faint tail, departing from the nucleus towards the south, which corresponds to an H α feature detected by Rampazzo et al. (2005) in a Fabry-Perot study of the galaxy.

4.2 The UV surface brightness profiles

To quantitatively describe the shape of the UV surface brightness profiles we use the Sersic law (Sersic 1968). The Sersic profile is a generalization of the de Vaucouleur law with $\mu(r) \sim r^{1/n}$, where n is a free parameter, named the Sersic index. The profile is thus sensitive to structural differences between ETGs and provides a better fitting to real galaxy profiles.

The Sersic $r^{(1/n)}$ description is suited to represent the family of ETGs surface brightness profiles: for $n = 1$ the formula describes a simple exponential profile, while for $n = 4$ it expresses the de Vaucouleurs law.

For profile fitting we use the formalism and the methods described in Caon et al. (1996). We adopt:

$$\mu(r) = A + B r^{1/n}$$

which is connected to the logarithmic form of the Sersic law

$$\mu(r) = \mu_e + c_n \left[\left(\frac{r}{r_e} \right)^{1/n} - 1 \right]$$

through the effective parameters $\mu_e = A + c_n$ and $r_e = (c_n/B)^n$. The estimate of both the above parameters is then model dependent.

In Table 4 we provide for each galaxy the value of n , the coefficient A and B of the interpolation, and the surface brightness interval μ_{start} (to avoid the influence of the PSF in the centre) and μ_{end} corresponding to the truncation of the profile when the error exceeds $0.3 \text{ mag arcsec}^{-2}$. An inner cut-off of 3 times the PSF provides a safe determination of n (see also Caon et al. 1996; Brown et al. 2003).

The n index with the smallest σ_{bf} scatter is selected and reported in Table 4. Caon et al. (1996) describe the uncertainty associated with the measure of n . They compute the variation of n , Δn , if the rms scatter of the (O-C) residual exceeds by 25% the value of the best fitting. For $n \leq 10$, $\Delta n \simeq 0.25n$ while for larger n the uncertainty may easily exceed 2, i.e. $n \pm 2$.

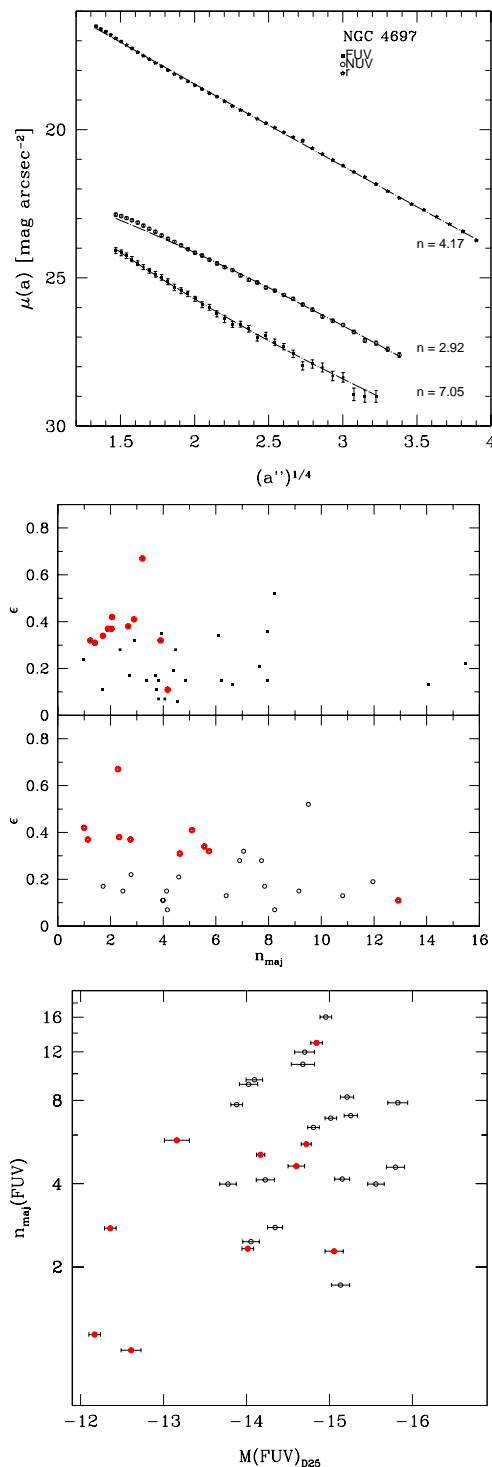


Figure 3. Top panel: example of fitting with a Sersic law of the observed optical and *GALEX* surface brightness profiles of NGC 4697 along the major axis. The index of the Sersic law, n , derived from the best fitting of the r (stars), of the NUV (open circles) and FUV (filled squares) surface brightness profiles is indicated. Middle panel: plot of the average ellipticity ϵ vs. n indices calculated in the NUV (top) and FUV (bottom) bands. Large red circles mark the S0 galaxies. Bottom panel: the FUV absolute magnitude integrated within the optical D_{25} diameter is plotted vs. n . Data are provided in Table 3 and Table 4

Table 3. FUV, NUV *GALEX* and SDSS *r* aperture photometry.

Ident.	FUV _{<i>r_e/8</i>} [AB mag]	NUV _{<i>r_e/8</i>} [AB mag]	FUV _{<i>r_e/4</i>} [AB mag]	NUV _{<i>r_e/4</i>} [AB mag]	FUV _{<i>D</i>25} [AB mag]	NUV _{<i>D</i>25} [AB mag]	<i>r_{r_e/8}</i> [AB mag]	<i>r_D25 [AB mag]</i>
NGC128	22.41±0.24	21.67±0.11	20.59±0.13	19.82±0.07	18.70±0.11	17.70±0.06		
NGC777	19.48±0.09	19.21±0.05	18.89±0.09	18.47±0.05	18.34±0.11	17.31±0.05		
NGC1052	19.19±0.08	18.48±0.04	18.47±0.07	17.68±0.04	17.37±0.07	16.12±0.04	12.53±0.02	10.36±0.01
NGC1209	21.60±0.16	20.86±0.07	19.92±0.11	19.07±0.05	18.49±0.10	17.22±0.04		
NGC1380	20.50±0.12	19.72±0.05	19.42±0.10	18.42±0.04	16.97±0.08	15.49±0.04		
NGC1389	22.22±0.08	20.85±0.04	20.92±0.07	19.38±0.04	18.78±0.07	16.93±0.03		
NGC1407	18.09±0.07	17.73±0.04	17.55±0.07	17.09±0.04	16.46±0.08	15.61±0.04		
NGC1426	21.28±0.15	19.92±0.06	20.23±0.12	18.83±0.05	18.60±0.11	16.87±0.05		
NGC1453	20.82±0.11	20.34±0.06	19.91±0.10	19.32±0.05	18.45±0.11	17.54±0.05		
NGC1521	21.50±0.19	20.14±0.07	20.73±0.16	19.23±0.06	19.30±0.22	17.34±0.05		
NGC1533	19.81±0.11	19.18±0.05	18.91±0.09	18.10±0.04	17.01±0.08	15.97±0.04		
NGC1553	18.70±0.08	17.39±0.04	17.98±0.07	16.58±0.04	16.62±0.07	14.46±0.03		
NGC2911	22.00±0.24	20.53±0.09	21.12±0.19	19.51±0.07	19.44±0.13	17.32±0.05	13.50±0.02	11.49±0.02
NGC2962	21.77±0.18	20.83±0.08	20.87±0.14	19.80±0.06	18.91±0.10	17.81±0.05	14.03±0.02	11.78±0.02
NGC2974	20.25±0.10	19.39±0.05	19.48±0.08	18.51±0.05	17.65±0.08	16.34±0.04		
NGC3258	19.68±0.10	19.48±0.06	18.91±0.09	18.10±0.04	18.19±0.14	17.07±0.06		
NGC3268	20.28±0.12	19.69±0.06	19.73±0.11	18.99±0.06	18.43±0.17	16.86±0.05		
NGC3489	19.29±0.09	17.88±0.04	18.68±0.08	17.21±0.04	16.86±0.07	15.13±0.04	12.41±0.02	10.14±0.01
NGC3607	18.66±0.07	17.89±0.04	17.61±0.06	16.84±0.04	16.65±0.07	15.38±0.04	12.07±0.02	9.94±0.01
NGC3818	21.07±0.15	20.11±0.08	20.23±0.12	19.10±0.06	19.16±0.14	17.41±0.05		
NGC3962	20.11±0.10	19.20±0.05	19.32±0.09	18.25±0.05	17.89±0.09	16.34±0.04		
NGC4374	18.35±0.08	17.59±0.04	17.61±0.07	16.76±0.04	16.32±0.07	15.13±0.03	11.48±0.01	9.52±0.01
NGC4552	17.95±0.07	17.86±0.04	17.24±0.07	16.94±0.03	16.17±0.07	15.20±0.03	12.29±0.02	9.39±0.01
NGC4697	18.73±0.08	17.43±0.04	18.04±0.08	16.61±0.04	16.58±0.08	14.83±0.04	11.34±0.01	9.35±0.01
NGC5011	21.69±0.21	20.41±0.08	20.74±0.17	19.33±0.07	22.25±0.54	17.19±0.06		
NGC5044	18.91±0.09	18.41±0.05	18.23±0.09	17.61±0.05	17.39±0.10	16.39±0.05		
NGC5363	18.83±0.06	18.28±0.03	18.08±0.06	17.32±0.03	17.03±0.06	15.71±0.03	12.60±0.02	9.87±0.01
NGC5638	20.93±0.14	19.86±0.06	20.04±0.11	18.68±0.05	18.49±0.10	16.79±0.04	13.57±0.02	11.19±0.02
NGC5813	19.78±0.09	18.77±0.05	19.11±0.08	17.99±0.04	18.22±0.10	16.84±0.04	14.95±0.04	10.85±0.01
NGC5831	21.11±0.13	20.09±0.05	20.29±0.11	19.11±0.04	18.95±0.13	17.16±0.04	13.60±0.02	11.22±0.02
NGC5846	18.88±0.09	18.28±0.05	18.11±0.08	17.43±0.04	17.12±0.09	15.95±0.04	12.29±0.02	10.07±0.02
NGC6868	20.16±0.11	19.26±0.06	19.26±0.09	18.31±0.05	18.05±0.12	16.41±0.05		
NGC6958	21.24±0.13	19.95±0.06	20.31±0.10	18.86±0.05	18.72±0.11	16.84±0.04		
NGC7079	21.84±0.18	20.02±0.07	21.10±0.14	19.24±0.06	19.49±0.15	16.97±0.04		
NGC7135	19.73±0.10	19.52±0.06	19.31±0.09	18.88±0.05	18.10±0.10	17.07±0.05		
NGC7192	21.09±0.15	19.87±0.06	20.19±0.12	18.85±0.05	18.53±0.11	16.98±0.04		
NGC7332	22.20±0.20	20.39±0.07	20.92±0.14	19.02±0.05	18.69±0.12	16.56±0.04	13.50±0.02	10.87±0.01
IC1459	18.39±0.07	18.04±0.04	17.75±0.07	17.25±0.04	16.49±0.07	15.45±0.04		
IC4296	19.56±0.10	18.84±0.06	18.82±0.09	18.00±0.05	17.68±0.12	16.34±0.05		
IC5063	20.60±0.10	19.61±0.05	19.79±0.09	18.72±0.05	18.17±0.09	17.05±0.04		

Note: Magnitudes are not corrected for galactic extinction.

In Table 4 we describe the quality of the whole fitting as judged by visual inspection. The profile quality is classified “poor” in the presence of distinct, intrinsic systematic deviations of the luminosity profile from the best fit Ser-sic law. When the fitting interval is too small (less than 3 mag/arcsec⁻²), the result is not reported in Table 4. We do not fit ETGs whose profiles are dominated by the presence of a ring, namely NGC 1533, NGC 2962, NGC 2974, IC 5063. In the case of NGC 3489 the fitting is quite poor, although fitting parameters are provided. The FUV surface brightness profiles are generally more noisy than those in the NUV band and the fitting results have higher uncertainties.

In Figure 3 (top panel) we plot an example of the Ser-sic fit in the FUV, NUV and *r* bands. We notice that the derived index *n* is significantly different in the three bands for some ETGs. Some large values of *n* are found also in optical bands where surface brightness profiles are best fit-

ted over a much larger magnitude range from the nucleus to the galaxy outskirts. For example, our largest Ser-sic index $n(FUV)=16.02$ of the shell galaxy NGC 4552, for which however we find $n = 4.5$ and 6 in NUV and *r*, is comparable to the Caon et al. (1996) value of $n_{maj}=13.87$ in the B band. For the same galaxy Kormendy et al. (2009) derive in the V band $n = 9.22^{+1.13}_{-0.83}$, which differs by $> 3\sigma$ from our *r* value. On the other hand, for NGC 4374, another slow rotator like NGC 4552 but without perturbation signatures (see Paper II on-line notes), we obtain $n \approx 6.5$ in all bands, consistent within the errors with $n = 7.9^{+0.71}_{-0.56}$ obtained by Kormendy et al. (2009) in the V-band.

The values of *n* in the UV bands range from 1 to 16 just as in the optical (e.g. Caon et al. 1996) and in the NIR (Brown et al. 2003) samples of ETGs. In our SDSS sample the range of *n* is smaller, from 2.55 to 9.41, comparable to the range of $n = 1.40\text{--}11.84$ obtained in the V band by

Kormendy et al. (2009) for a larger sample of Virgo galaxies. The median of the n distribution is 3.83, 5.09, 3.52 for NUV, FUV and r bands, while averages ($\pm 1\sigma$ errors) are 4.52 ± 3.16 , 5.96 ± 3.66 , 4.27 ± 1.95 , respectively.

The average galaxy ellipticity ϵ , does not correlate with the Sersic index (see Figure 3 middle panel), although more flattened galaxies tend to have lower values of n , as noticed by Caon et al. (1996). Lenticular galaxies, i.e. truly disk galaxies, tend to have n values typically lower than 5 in our sample.

In the bottom panel of Figure 3 we plot the absolute FUV magnitudes within the D_{25} aperture versus the n value from the FUV profile. The plot shows a weak correlation (correlation coefficient 0.350) and a rather large dispersion. The sense of the correlation is that n becomes larger with increasing total luminosity as observed in several samples. Brown et al. (2003) (their Figure 4), Coenda et al. (2005) (their Figure 9) found a large scatter when the n values are plotted vs. the total absolute K, R and V band magnitudes. A correlation, although weak, between n and the bulge K total absolute magnitude was found by Andredakis et al. (1995). Caon et al. (1996) and Prugniel et al. (1997) found that n and the absolute B, M_B , band magnitudes are significantly correlated. Prugniel et al. (1997) suggest that the non-homology, mapped by the Sersic index, may contribute to the tilt of the Fundamental Plane. They show that n correlates with the residual of the ETGs Fundamental Plane, i.e. that the non-homology in the ETGs structure has a measurable effect on their scaling relations.

Kormendy et al. (2009) parametrized the surface brightness profiles of Virgo Es with the Sersic law. They found that the dichotomy between core Es (generally slowly rotating, with a relatively high anisotropic velocity distribution and boxy isophotes) and ‘light Es’ (fast rotators, with disk isophotes) were also reflected in their Sersic index. Core Es tend to have $n > 4$ while ‘light Es’ have $n \simeq 3 \pm 1$. Kormendy et al. (2009) suggest that the two families of Es have a different origin since core Es tends to be α -enhanced relative to ‘light Es’.

In the top panel of Figure 4 we plot the average n index of a galaxy (the value and the error are obtained averaging over the UV and r bands) versus the corresponding measure of the α -enhancements within $r_e/8$ (column 10 in Table 1). ETGs with $n > 4$ tend to have $[\alpha/\text{Fe}]$ values larger than 0.15, while those with $n < 4$ span a wider range of $[\alpha/\text{Fe}]$, from ~ 0.04 to ~ 0.34 . This trend is confirmed if we consider the Sersic indices obtained from the r -band photometry. Galaxies with $n=3 \pm 1$ are mostly fast rotators, S0 galaxies. Among them there are the galaxies with the younger luminosity-weighted ages.

In the bottom panel of Figure 4 we plot the Sersic index versus the galaxy central velocity dispersion reported in Table 1. As reported in Section 2, the ETGs velocity dispersion is a proxy of the galaxy mass (Cappellari et al. 2006). The tight relation between the galaxy velocity dispersion and $[\alpha/\text{Fe}]$ is well described in Clemens et al. (2006, 2009, and reference therein), where it is shown that it is also independent from the galaxy environment, as well as the velocity dispersion vs. metallicity relation. Clemens et al. (2009) argue that the timing process of formation of ETGs is determined by the environment, while the details of the process of star formation, which has built up the stellar mass, are

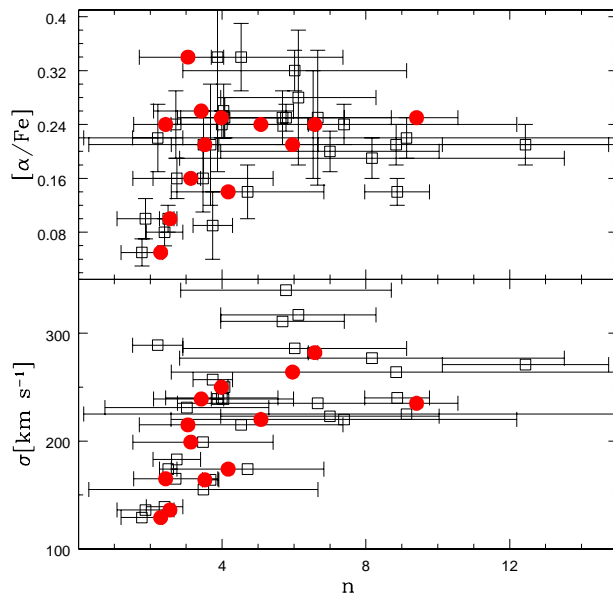


Figure 4. (*Top panel*) The Sersic index n vs. nuclear $[\alpha/\text{Fe}]$. Open squares indicate the values obtained averaging the Sersic indices derived in FUV, NUV and r . Filled dots are for the n values derived from the r -band alone. (*Bottom panel*) The average Sersic index n vs. the galaxy central velocity dispersion (Table 1).

entirely regulated by the halo mass. We suggest that the relation between the Sersic index, a global indicator of the galaxy structure, and $[\alpha/\text{Fe}]$ shown in Figure 4 likely reflects the more basic relation between this latter variable and the galaxy mass.

4.3 The UV radial colour profiles

Radial colour profiles provide information about the presence of age/metallicity gradients in the stellar populations. In Figure 5 we plot the (FUV-NUV) colour as a function a/r_e , where a is the semi-major axis and r_e is the optical effective radius. We stress that, while the UV colour profiles may extend out to several optical effective radii, the luminosity-weighted ages, metallicities and α -enhancements, derived in Paper III, refer to apertures whose radius is only a fraction of r_e .

In the upper panels of Figure 5 the (FUV-NUV) colour profiles of galaxies with a luminosity-weighted age lower than 4 Gyr are shown in the left panel and of galaxies older than 10 Gyr in the right panel, using age estimates from Paper III (see Table 1). Mean ages younger than 4 Gyr are likely due to recent star formation episodes superimposed on an old stellar population. We exclude from these panels ETGs with rings which we collect in the bottom right panel.

Figure 5 clearly shows that the (FUV-NUV) colour tends to become progressively redder from the centre outwards. This trend is consistent with the stellar populations becoming progressively more metal poor or younger (or a combination of both) with increasing distance from the galaxy centre. In fact, the NUV light is dominated by turnoff stars. On the other hand, the FUV emission of old ‘normal’ stellar populations is dominated by PAGB stars. As a popu-

Table 4. Result of the fit in the FUV and NUV *GALEX* and SDSS *r* bands

Ident.	n_{maj}^{FUV} n_{maj}^{NUV} n_{maj}^r	σ_{bf}	μ_{start}	μ_{end}	A	B	Quality
			[mag/arcsec ⁻²]	[mag/arcsec ⁻²]			
NGC 128	2.28	0.076	25.70	28.70	22.37	1.344	G
	3.21	0.044	25.03	28.50	19.59	23.29	G
NGC 777	4.59	0.118	26.60	28.70	16.52	5.775	P
	7.65	0.126	26.05	28.82	12.54	9.445	P
NGC 1052	7.73	0.073	25.70	29.2	12.26	9.760	F
	2.36	0.060	24.60	28.50	21.91	0.941	F
	3.05	0.034	17.40	23.80	14.14	2.090	G
NGC 1209	9.51	0.097	26.10	28.70	8.73	13.411	F
	8.23	0.050	25.00	28.50	11.47	9.893	G
NGC 1380	5.09	0.063	25.20	28.20	17.81	4.603	P
	2.89	0.071	24.20	29.10	20.50	1.441	G
NGC 1389	2.76	0.048	26.60	29.50	21.54	2.126	G
	2.04	0.090	25.30	29.30	21.89	0.897	G
NGC 1407	8.23	0.092	25.00	28.00	11.74	9.820	P
	3.82	0.043	24.70	27.80	19.81	2.429	F
NGC 1426	–	–	–	–	–	–	
	6.11	0.049	25.20	28.00	15.11	6.627	F
NGC 1453	1.72	0.104	26.20	28.40	23.37	0.675	P
	2.71	0.070	25.60	28.00	22.06	1.345	P
NGC 1521	–	–	–	–	–	–	
	2.97	0.054	25.60	28.00	21.09	1.836	G
NGC 1533	–	–	–	–	–	–	
	–	–	–	–	–	–	
NGC 1553	2.33	0.071	25.20	28.70	22.75	0.892	F
	2.67	0.092	24.10	28.10	21.12	1.052	G
NGC 2911	–	–	–	–	–	–	
	3.90	0.049	26.24	27.50	21.93	2.128	G
	9.41	0.050	18.54	24.50	5.94	10.893	F
NGC 2962	–	–	–	–	–	–	
	–	–	–	–	–	–	
	–	–	–	–	–	–	
NGC 2974	–	–	–	–	–	–	
	–	–	–	–	–	–	
	–	–	–	–	–	–	
NGC 3258	10.81	0.063	25.90	27.80	3.99	17.643	P
	14.07	0.070	25.69	28.11	1.46	19.971	P
NGC 3268	–	–	–	–	–	–	
	0.99	0.036	25.45	26.9	24.52	0.066	P
NGC 3489	1.14	0.196	25.28	29.00	23.82	0.130	P
	1.90	0.087	23.71	28.00	20.95	0.632	P
	2.29	0.136	16.70	24.00	14.51	1.272	F
NGC 3607	12.92	0.067	25.50	27.60	-1.47	21.61	P
	4.17	0.015	24.90	28.00	18.48	2.990	G
	5.08	0.035	17.18	23.30	10.78	4.879	G
NGC 3818	–	–	–	–	–	–	
	7.97	0.098	25.70	28.50	14.13	8.282	F
NGC 3962	2.78	0.115	26.20	28.30	21.51	1.898	P
	15.49	0.054	25.50	27.50	2.36	19.167	P
NGC 4374	6.39	0.072	25.00	28.50	14.84	6.844	G
	6.63	0.030	24.00	28.00	14.23	6.569	G
	6.58	0.029	16.60	23.00	8.19	6.801	G
NGC 4552	16.02	0.088	25.00	28.90	-6.24	26.813	F
	4.54	0.034	24.40	28.00	17.42	3.923	G
	5.96	0.043	17.00	25.00	8.49	6.697	G
NGC 4697	7.05	0.083	25.40	28.40	15.28	7.041	G
	2.92	0.032	24.00	27.20	20.82	1.287	G
	4.17	0.033	16.80	23.80	12.63	2.999	G
NGC 5011	–	–	–	–	–	–	
	7.96	0.082	25.45	27.00	13.27	8.72	F
NGC 5044	3.99	0.100	25.20	27.80	18.39	3.806	F
	3.75	0.037	25.20	27.3	19.98	2.500	G

Table 4. Continued

Ident.	n_{majFUV} n_{majNUV} n_{majr}	σ_{bf}	μ_{start}	μ_{end}	A	B	Quality
			[mag/arcsec ⁻²]	[mag/arcsec ⁻²]			
NGC 5363	5.56	0.107	25.20	30.00	16.42	5.789	P
	1.71	0.086	24.41	29.10	23.18	0.3250	P
	3.13	0.080	17.21	24.5	14.04	2.010	P
NGC 5638	3.99	0.180	26.95	29.40	21.37	2.927	P
	1.71	0.078	25.20	28.40	23.48	0.395	P
	2.43	0.077	18.17	24.80	15.76	1.405	G
NGC 5813	2.47	0.115	26.00	28.50	22.81	1.203	P
	6.22	0.048	25.20	28.30	17.190	5.158	F
	3.42	0.100	17.74	24.4	14.39	2.325	P
NGC 5831	—	—	—	—	—	—	
	3.84	0.068	25.50	28.70	19.65	2.913	G
	3.52	0.047	18.30	25.00	14.11	28.76	G
NGC 5846	4.16	0.128	25.40	28.80	17.64	4.179	P
	4.06	0.056	24.81	27.80	18.88	3.052	G
	3.98	0.027	17.90	23.40	13.76	2.882	G
NGC 6868	11.96	0.079	26.00	28.00	4.04	17.942	P
	4.38	0.035	25.20	27.80	18.86	3.349	G
NGC 6958	9.15	0.113	27.10	29.20	9.51	13.310	P
	4.85	0.084	25.40	28.00	18.06	4.203	F
NGC 7079	5.74	0.141	27.20	28.80	17.36	6.471	P
	1.23	0.081	25.20	29.20	24.23	0.137	P
NGC 7135	4.63	0.052	26.50	28.30	19.82	3.995	P
	1.41	0.099	25.80	28.80	24.69	0.183	P
NGC 7192	4.13	0.150	27.10	28.90	21.28	3.229	P
	3.35	0.087	25.60	28.80	20.38	2.367	F
NGC 7332	1.00	0.086	25.60	28.60	25.02	0.066	F
	2.06	0.046	23.70	28.20	20.93	0.758	F
	2.55	0.082	16.67	24.40	13.81	1.580	F
IC 1459	6.90	0.057	25.30	28.50	14.03	7.894	G
	4.47	0.033	24.65	28.00	18.48	3.410	G
IC 4296	7.85	0.101	26.50	28.43	12.17	10.203	P
	3.71	0.052	25.30	27.51	20.31	2.432	F
IC 5063	—	—	—	—	—	—	
	—	—	—	—	—	—	

lation gets younger or more metal poor, the turnoff becomes bluer and more luminous, and emits more in the NUV; at the same time, the contribution to the FUV from PAGB stars diminishes because, in spite of the higher luminosity, the duration of the PAGB phase gets much shorter (i.e., the fuel decreases). This causes the FUV-NUV colour to become redder. However, the situation could be more complex if ‘anomalous’ sub-populations, such as those suggested to be responsible for the UV-upturn of elliptical galaxies, were present. Several populations could develop hot horizontal branch (HHB) and AGB Manqué stars: very helium-rich stars such as those recently found in globular cluster multiple stellar populations (e.g. Piotto 2008); ultra metal-rich stars (Bressan et al. 1994; Bertola et al. 1995); or normal metallicity stars with enhanced mass loss (Yi et al. 1997). Such populations could contribute, if not dominate, the FUV light. The effects of such extreme populations will be the subject of a forthcoming investigation.

For populations younger than 1-2 Gyr (depending on the metallicity) this trend is inverted, since the turnoff starts to contribute significantly to the FUV band. Thus the (FUV-NUV) colour becomes steeply bluer with decreasing age. We

conclude that the FUV-NUV colour profile cannot be used alone to discriminate between negative age or metallicity gradients. We know however from studies based on absorption line indices that strong negative metallicity gradients are present in ETGs. Thus, the (FUV-NUV) colour trend may be, at least in part, due to a metallicity effect.

Three out of the five rejuvenated galaxies in the top left panel of Figure 5 (NGC 1521, NGC 6958, NGC 7332) display redder colours than the ‘old’ galaxies. We notice that the *GALEX* (FUV-NUV) colour is not very sensitive to reddening for Milky Way-type dust (an $E(B-V)=0.3$ implies a $\Delta m \approx 0.2$). Thus, if the red colours were due to a reddening effect, we should have an extinction as high as $E(B-V) \geq 0.5$. It is unlikely that such a strong extinction is present over several galaxy effective radii. For this reason, we interpret the observed colours as intrinsic. Lick indices do not show evidence for particularly low metallicities in the 5 galaxies. On the contrary, the metallicities are quite high in all but NGC 7332 consistent with their high velocity dispersions ($\sigma > 200 \text{ km s}^{-1}$). Thus, we suggest that the observed UV colours further support the presence of young luminosity-weighted ages in these galaxies.

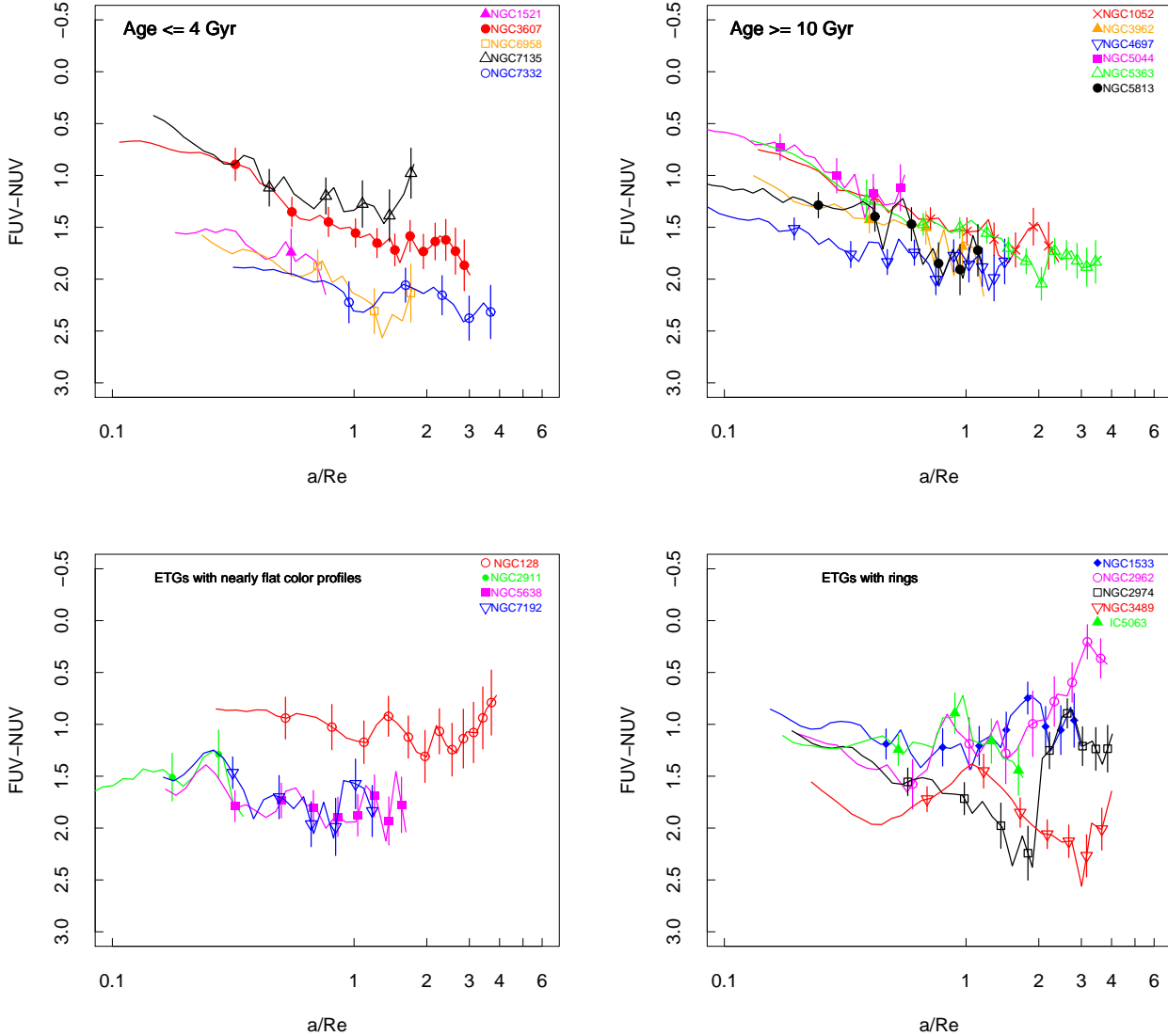


Figure 5. UV radial colour profiles normalized to the optical effective radius. In the top panel we plot the UV radial profiles of the rejuvenated and *old* ETGs according to the luminosity-weighted ages estimated from the line-strength index analysis developed in Paper III. The bottom left and bottom right panels isolate a set of ETGs with nearly flat UV radial profiles and the set of ETGs showing a ring-like structure.

In the bottom left panel of Figure 5 we plot separately the profiles of four galaxies, namely NGC 128, NGC 2911, NGC 5638 and NGC 7192. Their luminosity-weighted ages range from 5.7 ± 2.0 (NGC 7192 and NGC 2911) to 9.7 ± 1.7 Gyr (NGC 128) while their metallicities are solar or twice solar (NGC 2911 and NGC 7192), the latter with a correspondingly high central velocity dispersion. Their ($FUV-NUV$) colour profiles tend to be nearly flat. Three out of four of these galaxies show a very faint UV emission extending out to 2 optical r_e . Only the profile of NGC 128 extends up to 4 r_e and it is very similar to that of NGC 7332 (top left panel), although much bluer ($(FUV-NUV) \approx 1$) in the first galaxy vs. ≈ 2.2 in NGC 7332. Both galaxies are edge-on S0, with nearly solar metallicity.

In the right bottom panel of Figure 5, the colour profiles are characterized by the presence of blue rings, which appear as blue peaks in the ($FUV-NUV$) colours. As discussed at the beginning of this section, an abrupt blueing of the UV colours can be due to very recent star formation. Notice however the presence of both rejuvenated (NGC 3489) and old (NGC 1533, NGC 2974) nuclei as indicated by the luminosity-weighted ages derived in Paper III in the $r_e/8$ region.

We examined the behaviour of the central ($FUV-NUV$) colour vs. the ‘activity class’ (see Table 1, column 11). Although most of our galaxies have a LINER nuclei, Seyfert, Composite and Inactive nucleus are present (see Paper IV). We find that the central UV colour is to-

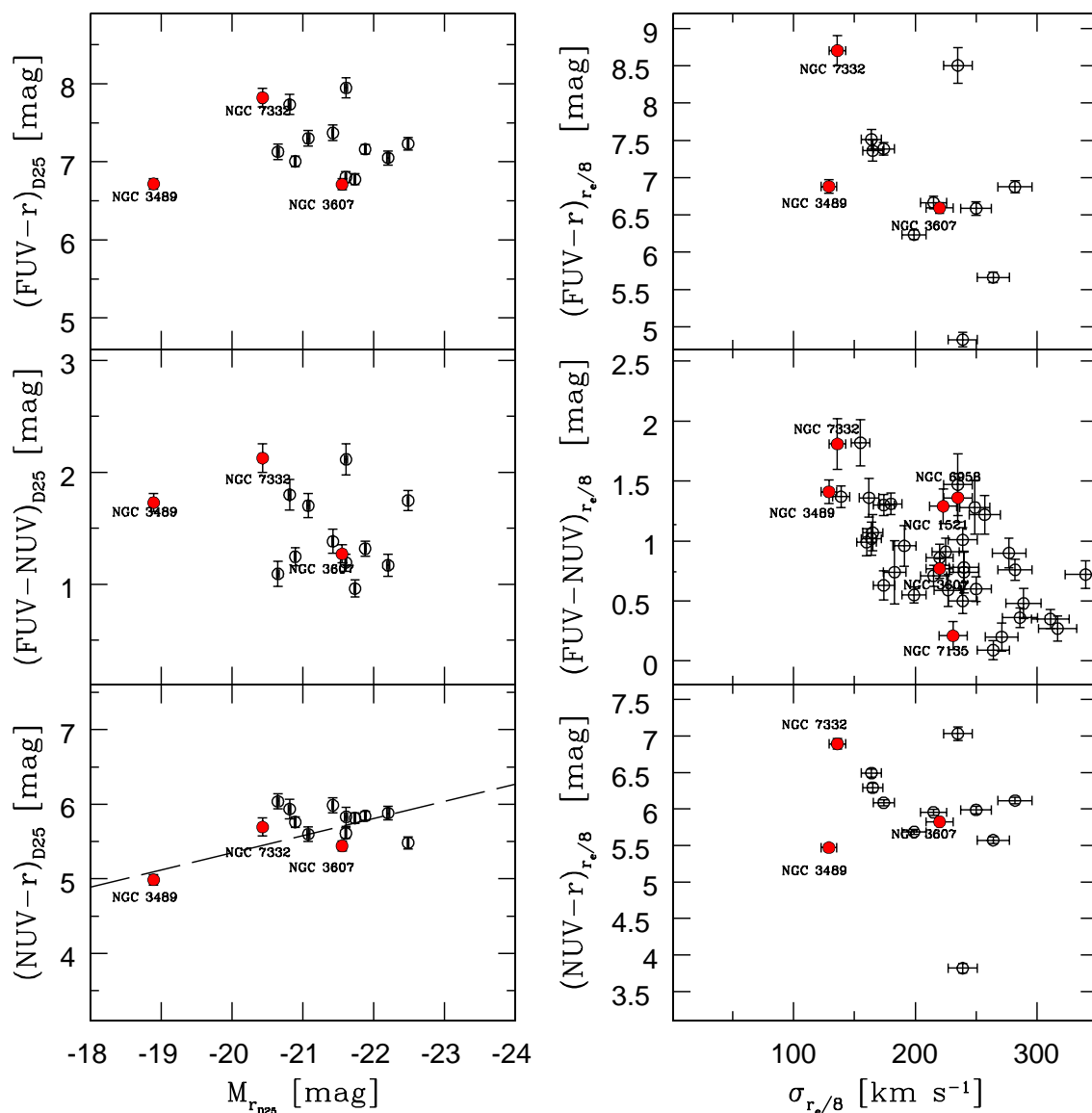


Figure 6. Left panels: UV - optical Color magnitude diagrams for a sub-sample of 14 galaxies with SDSS r-band observations. Magnitudes were computed within D_{25} (see Table 3). The long-dashed line is the fit to the red sequence at $0 < z < 0.05$ derived by Yi et al. (2005). Right panels: colours vs σ at $r_{s/8}$ for the whole sample (except NGC 2962) and for the 14 galaxies with SDSS data. Filled dots indicate ETGs whose luminosity-weighted age is $\lesssim 4$ Gyr from Table 1.

tally uncorrelated with the activity class. The bluest (FUV-NUV) colours are seen in NGC 3258 and NGC 4552 nuclei, classified in Paper IV as Composite, from diagnostic diagrams (Kewley et al. 2001, 2006). NGC 3258 (4.5 ± 0.08 Gyr) and NGC 4552 (6.0 ± 1.4) could have experienced a recent star formation event. A similar result is found by Suh et al. (2010) on a large ETG sample drawn from the SDSS DR6. Their analysis of the radial color gradient of ETGs, shows that the so-called blue-cored galaxies, possible rejuvenated ETGs, occupy both the star-formation and Seyfert regions in the classical [OIII]/H β vs. [NII]/H α BTP diagram (Baldwin et al. 1981). These authors suggest that most blue-cored ETGs have centrally concentrated star

formation and a smaller fraction could be associated with Seyfert activity.

4.4 Star formation and the large scale HI distribution

The FUV flux and the HI distributions correlate in star forming regions (see e.g. Neff et al. 2005; Thilker et al. 2005). In this context, we investigated in the literature the presence and the morphology of the large scale HI distribution in the present ETG sample.

Only a few objects have been observed. The HI content of NGC 1052 has been observed with the VLA by

van Gorkom et al. (1986). Their Figure 5 shows an irregular HI structure, elongated roughly perpendicularly to the galaxy major axis. In the southwest region of NGC 1052, the HI distribution shows what appears to be a tidal tail, suggesting that the gas may have been acquired about 10^9 years ago. We notice that in NGC 1052 there is no correlation between the HI distribution and the far UV emission. Similar cases of tail-like HI distributions, decoupled from the Far UV emission, have been detected in some shell galaxies, namely NGC 2865, NGC 5018 and NGC 7135 (Rampazzo et al. 2007).

Werk et al. (2010) show the large scale HI distribution in the field of NGC 1533, one of our ETGs showing a blue outer ring. The HI distribution is connected to a companion galaxy, IC 2038. Four outer-HII regions are detected, powered by young, low mass OB associations according to Werk et al. (2010) (see their Figure 7). Their FUV-NUV colour, in the range $-0.79 \pm 0.37 \leq (FUV - NUV) \leq 0.03 \pm 0.28$, is bluer than the knotty regions in the galaxy ring, which we will discuss and model in a forthcoming paper (Marino et al. 2010).

The HI distribution has been investigated also in NGC 4374 (Li & van Gorkom 2001) and in NGC 5846 (Zabludoff et al. 2001). HI is detected in neither, although both have HI rich companions.

4.5 UV-optical colour vs. absolute magnitude and velocity dispersion relations

The left panels of Fig. 6 present UV-optical colour-magnitude relations (CMRs) of the 14 galaxies for which SDSS data are available (see Table 3 and Appendix B). Magnitudes were computed within D_{25} . No clear correlations are observed in the (FUV-NUV) vs M_r and (FUV-r) vs M_r planes, while in the (NUV-r) vs M_r plane the positive trend is mainly driven by one object (NGC 3489) at relatively faint magnitudes. In this plane, our galaxies are consistent with the local universe ($0 < z < 0.05$) red sequence derived by Yi et al. (2005) ($-0.23 \pm 0.30 \times M_r + 0.75$). We also notice that rejuvenated galaxies are mixed with older ETGs in these CMRs.

In the right panels of Fig. 6, we plot the UV-optical colours derived within $r_e/8$ versus the central velocity dispersion $\sigma_{r_e/8}$. A significant correlation is observed only in the FUV-NUV vs σ plane, but in this case the sample is larger (39 galaxies). The Spearman correlation coefficient is $r_s = -0.62$ with $N=37$ degrees of freedom, indicating that an anti-correlation exists with a probability > 0.99 . This result is in agreement with Donas et al. (2007); Jeong et al. (2009).

Studies based on narrow-band indices have shown that the stellar populations in ETGs tend to become progressively more metal rich and older with increasing velocity dispersion (i.e., increasing galaxy mass) (e.g Thomas et al. 2005; Clemens et al. 2006, 2009). Both effects could be responsible for the observed FUV-NUV trend since in general this colour becomes bluer for more metal rich and older passive populations (see discussion in Section 4.3).

5 SUMMARY AND CONCLUSIONS

We have obtained *GALEX* NUV and FUV aperture and surface photometry of 40 ETGs whose emission line properties have been presented in Paper III and Paper IV. In Appendix B we also provide the SDSS *r*-band surface photometry of 14 of the above ETGs.

We used UV and optical imaging to study mechanisms driving both secular and/or external ETG evolution such as bars and recent accretion episodes, respectively, as suggested by the young luminosity-weighted ages resulting from the line strength indices analysis (see Paper III).

We find the following results:

1. In general, the (FUV-NUV) radial profiles become redder with galactocentric distance (see also Jeong et al. 2009). This property is common to both rejuvenated ($\lesssim 4$ Gyr) and old ETGs. The trend could be due to age and/or metallicity gradients. The presence of strong metallicity gradients in these ETGs as revealed by the analysis of narrow-band indices in Paper III suggests that the radial (FUV-NUV) profiles are due, at least in part, to radial metallicity variations. The role of the metallicity could be dominant if, as found by Clemens et al 2009, the age increases with galactocentric distance. The study of moderate redshift ($0.4 < z < 1.5$) ETGs performed by GOODS (Great Observatory Origins Deep Survey) (Ferrerias et al. 2009) suggest that redshift evolution of the observed color gradients is incompatible with a significant variation in stellar age within each galaxy and that the local observations of radial color gradients mostly correspond to a range of metallicities.
2. Relevant exceptions to what seems the ‘normal’ (FUV-NUV) colour profile are ring/arm-like galaxies. The NUV and FUV images of NGC 1533, NGC 2962, NGC 2974, NGC 3489 and IC 5063 show that ring and/or arm-like structures are bluer than the galaxy body. Kinematical models suggest that rings have an internally driven origin and are closely associated with the evolution of the bar. The gas may be driven both in the centre and in the ring region where accumulates and may activate star formation. The young luminosity-weighted age of NGC 3489 and its AGN-like activity may be explained in the framework of a gas inflow toward the galaxy centre. In Paper IV we found evidence that star formation and AGN activity are closely connected in time. We interpret the abrupt blueing of the UV colour in the ring/armlike structure as due to recent star formation. Detailed models are planned in a subsequent work. We consider these ETGs as possible candidates of ongoing secular evolution.
3. Shell galaxies are a prototypical example of the externally driven evolution of ETGs. Out of the seven ETGs in the sample with stellar shells detected in the optical, NGC 7135 is the only shell galaxy showing a shell structure in the NUV and FUV images. Rampazzo et al. (2007) suggest that this galaxy could have had a recent nuclear star formation episode as implied by the low luminosity-weighted age, likely triggered by the accretion event that formed the shell.
4. The Sersic profile shape parameter n shows much variation in UV ($1 < n < 16$) as in the optical and near infrared bands. S0s tend to have values of $n < 5$ in both NUV and FUV, as already noticed in the optical. The Sersic index $n = 4$ is a sort of watershed as noted in the optical by

Kormendy et al. (2009). Most ETGs with $n > 4$ have $[\alpha/\text{Fe}] \geq 0.15$, implying a short star-formation time scale. ETGs with $n=3\pm1$ have a large spread in $[\alpha/\text{Fe}]$, including very low values indicative of a more prolonged star formation. Most of these galaxies are S0s, i.e. truly disk galaxies, which, as noticed in Paper III, generally appear more rejuvenated with respect to Es. These galaxies have also, in general, a low central velocity dispersion. We suggest that the Sersic index vs. $[\alpha/\text{Fe}]$ trend reflects the velocity dispersion (i.e. mass) α -enhancement relation.

5. A significant correlation between the (FUV–NUV) colour and σ is observed, in agreement with previous studies (Donas et al. 2007; Jeong et al. 2009). This trend is likely to be driven by a combined effect of the age- σ and metallicity- σ relations found from narrow band indices. A more detailed investigation on the origin of this relation will be performed in a forthcoming paper.

A detailed analysis of the UV colour vs. line-strength indices and of the ETGs Spectral Energy distribution from UV to optical and MIR will be presented in forthcoming papers.

ACKNOWLEDGMENTS

We acknowledge Mauro D’Onofrio for his support, valuable discussions and comments. AM acknowledges support from Italian Scientist and Scholars in North America Foundation (ISSNAF) through an ISSNAF fellowship in Space Physics and Engineering, sponsored by Thales Alenia Space. RR, AB, FA, LMB acknowledge the ASI-INAF support through contract I/016/07/0. *GALEX* is a NASA Small Explorer, launched in April 2003. *GALEX* is operated for NASA by California Institute of Technology under NASA contract NAS-98034. This work was partly supported by NASA grant NNX07APO8G. This research has made use of SAOImage DS9, developed by Smithsonian Astrophysical Observatory and of the NASA/IPAC Extragalactic Database (NED) which is operated by the Jet Propulsion Laboratory, California Institute of Technology, under contract with the National Aeronautics and Space Administration. IRAF is distributed by the National Optical Astronomy Observatories, which are operated by the Association of Universities for Research in Astronomy, Inc., under cooperative agreement with the National Science Foundation. We acknowledge the usage of the HyperLeda database (<http://leda.univ-lyon1.fr>).

Facilities: *GALEX*, SDSS

REFERENCES

Adelman-McCarthy, J.K., Agüeros, M.A., Allam, S.S., Al-
lende Prieto, C., Anderson, K. S. J. et al. 2008, ApJS,
175, 297
Andredakis, Y.C., Peletier, R.F., Balcells, M. 1995, MN-
RAS, 275, 874
Annibali, F., Bressan, A., Rampazzo, R., Zeilinger, W.W.
2006, AA, 445, 79: Paper II
Annibali, F., Bressan, A., Rampazzo, R., Zeilinger, W.W.,
Danese, L. 2007, AA, 463, 455: Paper III
Annibali, F., Bressan, A., Rampazzo, R., Zeilinger, W.W.,
Vega, O., Panuzzo, P. 2010, AA, submitted: Paper IV

Athanassoula, E. 2009, in "Galaxies in Isolation: Exploring
Nature vs. Nurture" (2009arXiv0910.5180A)
Baldwin, J. A., Phillips, M. M., Terlevich, R. 1981, PASP,
93, 5
Bertola, F., Bressan, A., Burstein, D., Buson, L. M., Chiosi,
C., & di Serego Alighieri, S. 1995, ApJ, 438, 680
Bianchi, L. et al. 2007, in "Galaxy Evolution across the
Hubble Time" IAU Sympo. 235, F. Combes and J. Palous
eds., p. 301
Bianchi, L. 2009, Ap&SS, 320, 11
Bournaud, F., Combes, F., Semelin, B. 2005, MNRAS, 364,
L18
Bressan, A., Chiosi, C., Fagotto, F. 1994, ApJS, 94, 63
Brown, R.J.N., Forbes, D.A., Silva, D., Helsdon, S.F., Pon-
man, T.J. et al. 2003, MNRAS, 341, 747
Burstein, D., Bertola, F., Buson, L.M., Faber, S.M., Lauer,
T.R. 1988, ApJ, 328, 440
Buta, R., Combes, F. 1996, Fundamentals of Cosmic
Physics, Volume 17, 95.
Caon, N., Capaccioli, M., D’Onofrio, M. 1993, MNRAS.
265, 1013
Cappellari, M. et al. 2006, MNRAS, 366, 1126
Cardelli, J.A., Clayton, G.C., Mathis, J.S. 1989, ApJ, 345,
245
Chapman, S. C., Smail, I., Blain, A. W., Ivison, R. J. 2004,
ApJ, 614, 671
Clemens, M. S., Bressan, A., Nikolic, B., Alexander, P.,
Annibali, F., & Rampazzo, R. 2006, MNRAS, 370, 702
Clemens, M. S., Bressan, A., Nikolic, B., Rampazzo, R.
2009, MNRAS, 392, L35
Coenda, V., Donzelli, C.J., Muriel, H., Quintana, H., In-
fante, L., Lambas, D.G. 2005, AJ, 129, 1237
Colbert, J.W., Mulchaey, J.S., Zabludoff, A.I. 2001, AJ,
121, 808
De Lucia, G. Springel, V. White, S.D. M., Croton, D.
Kauffmann, G. 2006, MNRAS, 366, 499
de Vaucouleurs, G., de Vaucouleurs, A., Corwin, H.G. Jr.
et al. 1991 *Third Reference Catalogue of Bright Galaxies*,
Springer-Verlag, New York
Donas, J. Deharveng, J.-M., Rich, R.M., Yi, S.K., Lee, Y-
W, et al. 2007, ApJS, 173, 597
Ebeling, H., White, D. A., Rangarajan, F. V. N. 2006, MN-
RAS, 368, 65
Emsellem, E., Cappellari, M., Krajnović, D., van de Ven,
G., Bacon, R., et al. 2007, MNRAS, 379, 401.
Ferrerias, I., Lisker, T., Pasquali, A., Kaviraj, S. 2009, MN-
RAS, 395, 554
Franx, M., Labbé, I., Rudnick, G., van Dokkum, P.G.,
Daddi, E. et al. 2003, ApJ, 587, L79
Gil de Paz A. Boissier, S. Madore, B.F., Seibert, M.J.,
Young H.; Boselli, A. et al. 2007, ApJS, 173, 185
Goudfrooij, P. 1999, in *Star Formation in Early-Type
Galaxies*, ASP Conference Series 163, eds. J. Cepa and
P. Carral, 55
Grossi, M., di Serego Alighieri, S., Giovanardi, C. et al.
2009, A&A, 498, 407
Heckman, T. M. 1980, A&A, 87, 152
Kewley L. J., Dopita, M.A., Sutherland, R.S., Heisler,
C.A., Trevena, J., 2001, ApJ, 556, 121
Kewley, L. J., Groves, B., Kauffmann, G., & Heckman, T.
2006, MNRAS, 372, 961
Kormendy, J. 2004, ARA&A, 42, 603

- Kormendy, J., Fisher, D. B., Cornell, M. E., & Bender, R. 2009, *ApJS*, 182, 216
- Krajnović, D., Cappellari, M., Emsellem, E., McDermid, R.M., de Zeeuw, T.P. 2005, *MNRAS*, 357, 1113
- Jedrzejewski, R., 1987, *MNRAS*, 226, 747
- Jeong, H., Bureau, M., Yi, S., Krainović, D., Davies, R.L. 2007, *MNRAS*, 376, 1021
- Jeong, H., Yi, S., Bureau, M., Davies, R., Falcón-Barroso, J. et al. 2009, *MNRAS*, 398, 2028
- Laurikainen, E., Salo, H., Buta, R., Speltinckx, T., Block D. 2006, *AJ*, 132, 2634
- Li, Y., van Gorkom, J.H. 2001 in *Gas & Galaxy Evolution*, J.E. Hibbard, M.P. Rupen, and J.H. van Gorkom eds., ASP Conf. Ser., Vol 240, pag. 637
- Macchetto, F., Pastoriza, M., Caon, N., Sparks, W.B., Gavalisco, M. et al. 1996, *AAS* 120, 463
- Malin, D.F., Carter, D. 1983, *ApJ*, 274, 534
- Marino, A., Iodice, E., Tantalò, R., Piovan, L., Bettoni, D., et al. 2009, *A&A*, 508, 1235
- Marino, A., Bianchi, L., Rampazzo, R. et al. 2010, to appear in “UV Universe 2010” Proceedings, St. Petersburg June, 2010
- Martin, D.C., Fanson, J., Schiminovich, D. et al. 2006, *ApJ*, 619, L1
- McDermid, R.M., Bacon, R., Kuntschner, H., Emsellem, E. Shapiro, K.L. et al. 2006, *New AR*, 49, 521
- Morrissey, P., Conroy, T., Barlow, T.A., et al. 2007, *ApJS*, 173, 682
- Neff, S. G., Thilker, D. A., Seibert, M., Gil de Paz, A., Bianchi, L., et al. 2005, *ApJ*, 619, L91
- Phillips, M., Jenkins, C., Dopita, M., Sadler, E.M., Binette, L. 1986, *AJ*, 91, 1062
- Piotto, G. 2008, *Memorie della Societa Astronomica Italiana*, 79, 334
- Prugniel, Ph., Simien, F. 1997, *AA*, 321, 111
- Rampazzo R., Annibali F., Bressan A., Longhetti M., Padoan F., Zeilinger W.W. 2005, *AA* 433, 497: Paper I
- Rampazzo, R., Marino, A., Tantalò, R., Bettoni, D., Buson, L. M., Chiosi, C., Galletta, G., Grützbauch, R., Rich, R. M. 2007, *MNRAS*, 381, 245
- Reduzzi, L., Longhetti, M., Rampazzo, R. 1996, *MNRAS*, 282, 149
- Rogers, B., Ferreras, I. Lahav, O., Bernardi, M., Kaviraj, S. Yi, S.K. 2007, *MNRAS*, 382, 750
- Sandage, A.R., Brucato, R. 1979, *AJ*, 84, 472
- Sandage, A.R., Tammann, G. 1987, *A Revised Shapley Ames Catalogue of Bright Galaxies*, Carnegie, Washington (RSA)
- Sarzi, M., Falcón-Barroso, J., Davies, R.L., Bacon, R. et al. 2006, *MNRAS*, 366, 1151
- Schawinski, K., Kaviraj, S., Khochfar, S., Yoon, S.-J., Yi, S. K. et al. 2007, *ApJS*, 173, 512
- Sersic, J. L. 1968, *Atlas de Galaxias Australes*, Observatorio Astronomico, Cordoba
- Suh, H., Jeong, H., Oh, K., Yi, S., Ferreras, I., Schawinski, K. 2010, *ApJ*, 187, 374
- Tal, T. van Dokkum, P.G., Nelan, J., Bezanson, R. 2009, *AJ*, 138 1417
- Terlevich, E., Diaz, A.I., Terlevich, R. 1990, *Revista Mexicana de Astronomia y Astrofisica*, 21, 218
- Thilker D.A., Bianchi, L., Meurer, G., Gil de Paz, A. Boissier, S. et al. 2007, *ApJS*, 173, 538
- Thilker, D. A., et al. 2005, *ApJ*, 619, L79
- Thomas, D., Maraston, C., Bender, R., & Mendes de Oliveira, C. 2005, *ApJ*, 621, 673
- Treu, T., Ellis, R.S., Liao, T.X., van Dokkum, P.G. 2005, *ApJ*, 622, L5
- Tully, R.B. 1988, *Nearby Galaxy Catalogue*, Cambridge University Press
- van Gorkom, J.H., Knapp G.R., Raimond, E., Faber, S.M., Gallagher, J.S. 1986, *AJ*, 91, 791
- Wada, K. 2004, in *Coevolution of Black Holes and Galaxies*, ed. L.C. Ho, Cambridge Univ. Press, 186
- Werk, J.K., Putman, M.E., Meurer, G.R., Ryan-Weber, E.V., Kehrig, C. et al. 2010, *AJ*, 139, 279
- Yan, R., Newman, J. A., Faber, S. M., Konidaris, N., Koo, D., & Davis, M. 2006, *ApJ*, 648, 281
- Yi, S., Demarque, P., & Oemler, A., Jr. 1997, *ApJ*, 486, 201
- Yi S.K., Yoon, S.-J., Kaviraj, S., Deharveng, J.-M., Rich, R. M., et al. 2005, *ApJ*, 619, L111
- Zabludoff, A. 2001 in *Gas & Galaxy Evolution*, J.E. Hibbard, M.P. Rupen, and J.H. van Gorkom eds., ASP Conf. Ser., Vol 240, pag. 547

APPENDIX A: UV AND SDSS DESCRIPTION OF INDIVIDUAL GALAXIES

We briefly comment here on the *GALEX* and SDSS surface brightness profiles of the ETGs presented in this paper. We also list morphological and kinematic peculiarities which could be relevant for understanding the galaxy evolution. For a detailed information about the luminosity-weighted age, metallicity and α -enhancements as well as about emission line properties we cross-refer to Papers III and Papers IV (these data are summarized in Table 1). The basic information about ETGs is provided in Papers I, II (on line material) and IV (Appendix A).

NGC 128 This edge-on S0 is a LINER. The (FUV-NUV) colour profile is flat within the errors (average $\approx 1.02 \pm 0.14$). The average Sérsic index is $\langle n_{ave} \rangle = 2.74 \pm 0.66$. Gas and stars counter rotate in this about 10 Gyr old fast rotator.

NGC 777 The (FUV-NUV) colour profile drops from ≈ 0.5 in the centre of the galaxy to ≈ 1.5 in the outskirts. This slow rotator, Seyfert-like galaxy has a young (5.4 ± 2.1) luminosity-weighted age in the nucleus. The average Sérsic index is $\langle n_{ave} \rangle = 6.14 \pm 2.16$: the quality of the fit is indeed quite poor.

NGC 1052 This old (≈ 14 Gyr), fast rotating galaxy is considered a prototypical LINER. A gas vs. gas counter rotation is reported for this galaxy. As in previous galaxy the (FUV-NUV) colour profile becomes red going from the centre (≈ 0.75) to the outskirts (≈ 1.75). (NUV-*r*) becomes slightly bluer from ≈ 0.55 to 0.5 while (FUV-*r*) redder from the centre ≈ 6.2 to 6.9. The average Sérsic index is $\langle n_{ave} \rangle = 4.53 \pm 2.83$. The large spread in the *n* indices does not depend from the quality of the fit.

Appendix A is available in its entirety in the online edition of the Journal. A small portion is shown here for guidance.

**APPENDIX B: SDSS SURFACE PHOTOMETRY
OF A GALAXY SUB-SAMPLE**

Figure A1 displays composite SDSS images available for 14 ETGs in our sample. Figure A2 shows the surface brightness profiles in the r band and the (FUV- r) and (NUV- r) colour profiles.

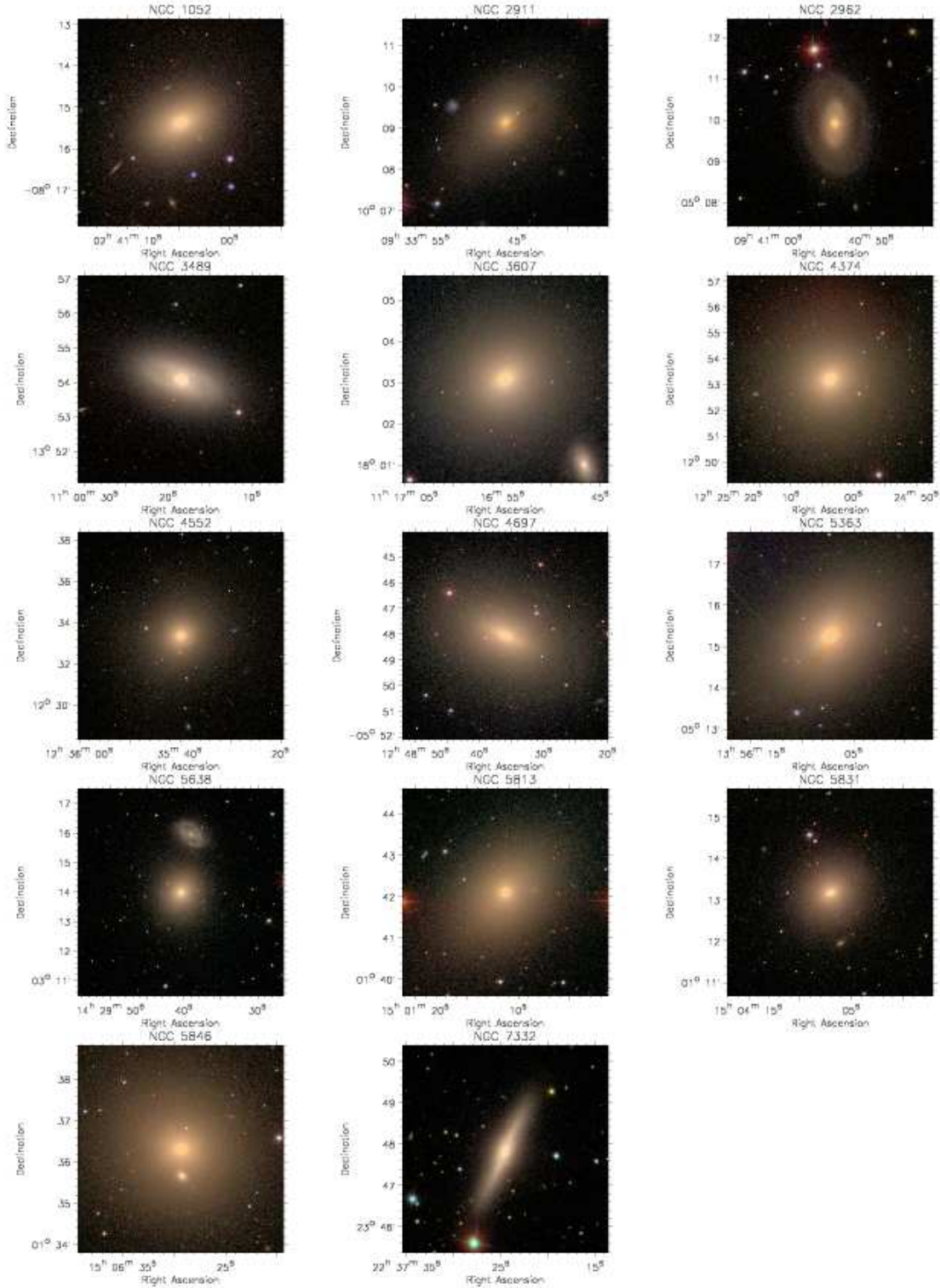


Figure B1. False colour composite SDSS images (*g* blue, *r* green, *i* red) available for 14 ETGs of the sample.

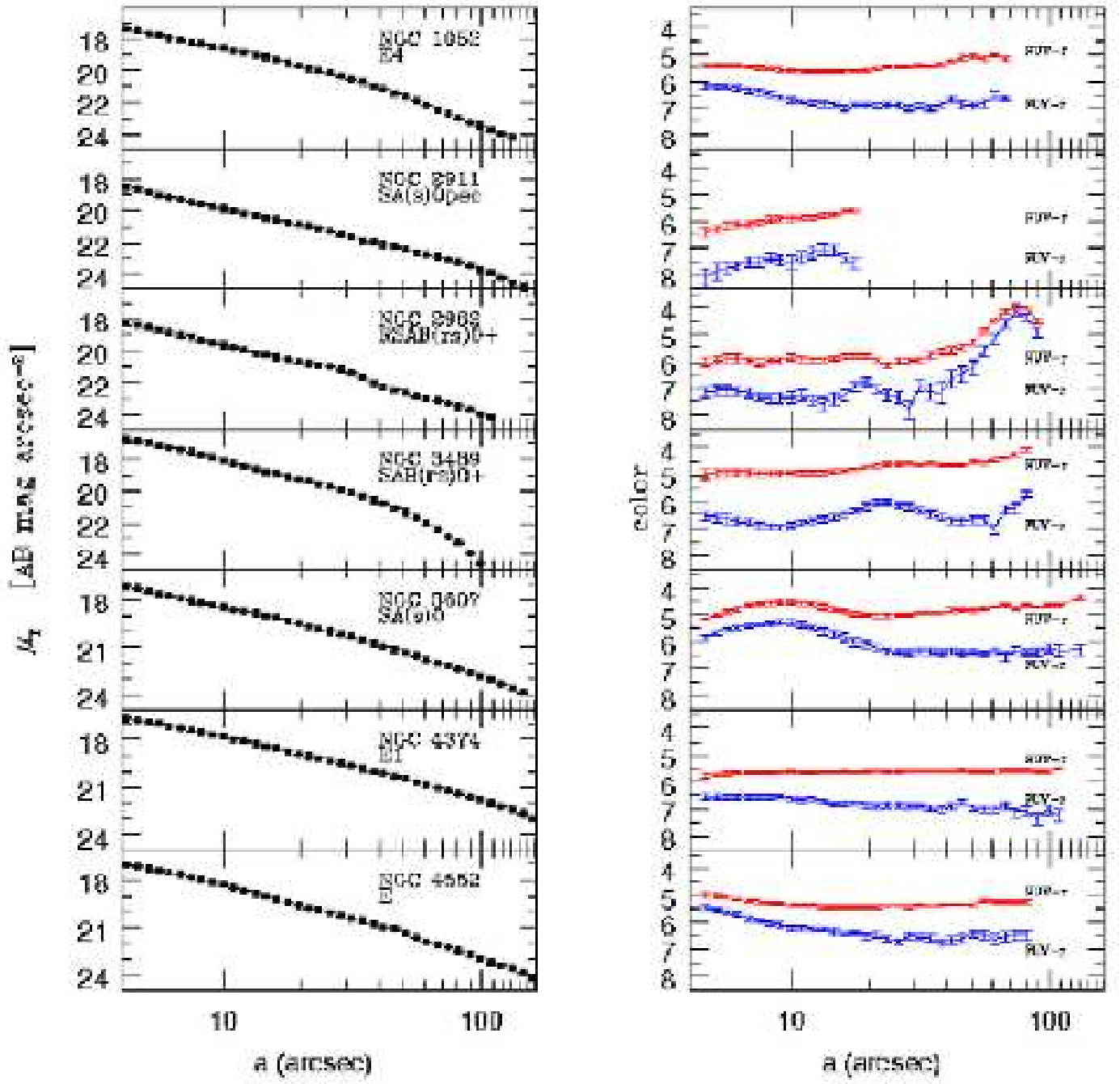


Figure B2. From top to bottom: (left panels) Luminosity profiles in the SDSS r band, (right panels) (FUV- r) and (NUV- r) colour profiles along the semi-major axis of the fitted ellipse.

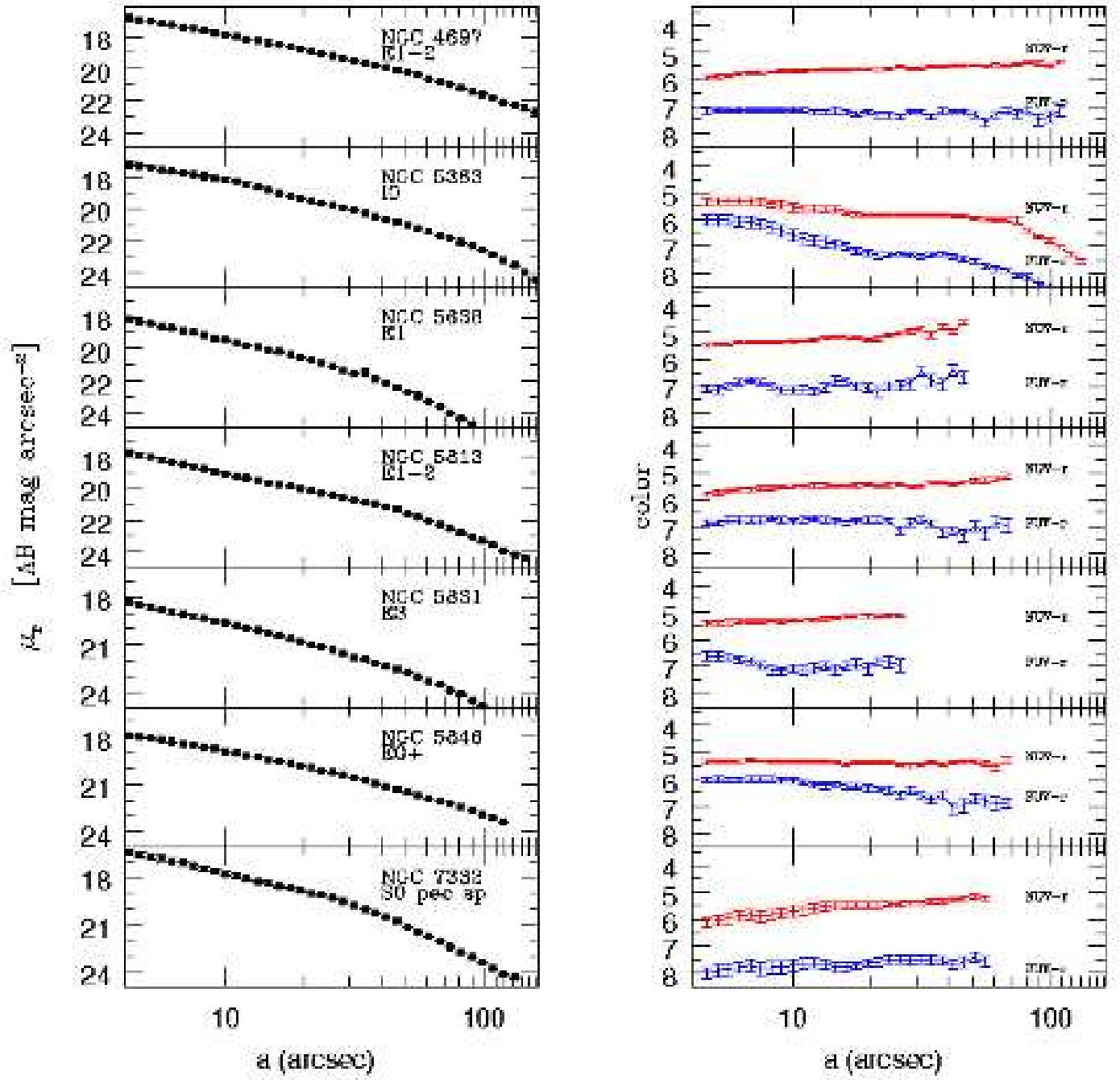


Figure B2. Continued.